Atmos. Chem. Phys., 7, 781–801, 2007
www.atmos-chem-phys.net/7/781/2007/

Atmospheric Chemistry and Physics

Modelling constraints on the emission inventory and on vertical dispersion for CO and SO_2 in the Mexico City Metropolitan Area using Solar FTIR and zenith sky UV spectroscopy

B. de Foy[1,*], W. Lei[2], M. Zavala[2], R. Volkamer[3], J. Samuelsson[4], J. Mellqvist[4], B. Galle[4], A.-P. Martínez[5], M. Grutter[6], A. Retama[7], and L. T. Molina[1,2]

[1]Molina Center for Energy and the Environment, La Jolla, USA
[2]Department of Earth, Atmospheric and Planetary Sciences, Massachusetts Institute of Technology, USA
[3]Department of Chemistry and Biochemistry, University of California, San Diego, USA
[4]Department of Radio and Space Science, Chalmers University of Technology, Gothenburg, Sweden
[5]General Direction of the National Center for Environmental Research and Training (CENICA), National Institute of Ecology (INE), Mexico
[6]Centro de Ciencias de la Atmósfera, Universidad Nacional Autónoma de México, Mexico
[7]Secretaría del Medio Ambiente, Gobierno del Distrito Federal, Mexico
[*]now at: Saint Louis University, USA

Received: 19 June 2006 – Published in Atmos. Chem. Phys. Discuss.: 11 July 2006
Revised: 8 January 2007 – Accepted: 9 February 2007 – Published: 14 February 2007

Abstract. Emissions of air pollutants in and around urban areas lead to negative health impacts on the population. To estimate these impacts, it is important to know the sources and transport mechanisms of the pollutants accurately. Mexico City has a large urban fleet in a topographically constrained basin leading to high levels of carbon monoxide (CO). Large point sources of sulfur dioxide (SO_2) surrounding the basin lead to episodes with high concentrations. An Eulerian grid model (CAMx) and a particle trajectory model (FLEXPART) are used to evaluate the estimates of CO and SO_2 in the current emission inventory using mesoscale meteorological simulations from MM5. Vertical column measurements of CO are used to constrain the total amount of emitted CO in the model and to identify the most appropriate vertical dispersion scheme. Zenith sky UV spectroscopy is used to estimate the emissions of SO_2 from a large power plant and the Popocatépetl volcano. Results suggest that the models are able to identify correctly large point sources and that both the power plant and the volcano impact the MCMA. Modelled concentrations of CO based on the current emission inventory match observations suggesting that the current total emissions estimate is correct. Possible adjustments to the spatial and temporal distribution can be inferred from model results. Accurate source and dispersion modelling provides feedback for development of the emission inventory, verification of transport processes in air quality models and guidance for policy decisions.

Correspondence to: B. de Foy
(bdefoy@mce2.org)

1 Introduction

Detailed and accurate emission inventories are a cornerstone of effective air quality management programs. Public policy choices can be evaluated with air quality models based on actual emissions and alternative scenarios in combination with accurate meteorological simulations. This paper makes use of novel measurement techniques to evaluate the carbon monoxide (CO) inventory for the Mexico City Metropolitan Area (MCMA) and to evaluate the potential impacts of large point sources of sulfur dioxide (SO_2). Even though vertical dispersion has a large impact on pollutant transport, it can be overlooked as a source of uncertainty. Pollution observations and simulations are further used to evaluate alternative vertical dispersion schemes.

1.1 Mexico City Metropolitan Area

Megacities are home to a growing number of people and can suffer from high levels of air pollution (Molina and Molina, 2004; Molina et al., 2004). The MCMA is a megacity of

Published by Copernicus GmbH on behalf of the European Geosciences Union.

around 20 million people living in a basin 100 km in diameter at 2240 m altitude and 19° N latitude. The basin is surrounded by high mountains on the west, south and east. There is intense solar radiation and high ozone levels most of the year. There has been extensive scientific study of the air quality in the MCMA, as reviewed in Molina and Molina (2002).

Nickerson et al. (1992) carried out aircraft profiles of ozone, SO_2 and particulate matter (PM) above Mexico City in 1991, highlighting the importance of combustion sources for the basin air pollution. Williams et al. (1995) modelled air dispersion for the same episodes looking at the transport of contaminants towards the southwest of the basin and emphasizing the need for improved accuracy of the emission inventory. Elliott et al. (1997) analysed the importance of liquefied petroleum gas (LPG) components in the urban air chemistry. By estimating CO residence times of approximately 2 days in the basin, estimates are made of the LPG venting to the regional environment.

Fast and Zhong (1998) developed a wind circulation model for the basin from data obtained during the IMADA campaign of 1997. This emphasized the importance of vertical mixing and mountain winds in the transport of the urban plume first towards the south and then back over the city to the north. Similar patterns are described in Jazcilevich et al. (2003) with evidence of direct convective transport from layers aloft to the surface.

MCMA-2003 was a major field campaign that took place in April 2003. De Foy et al. (2005) reviewed wind circulation patterns in the basin and classified the meteorological conditions into 3 episode types. O3-South are days when ozone is high in the south and a weak late afternoon jet flow forms. O3-North days are when the ozone peak is in the north due to the combination of a strong jet and flow over the south and west edges of the basin. Cold Surge days are when cold northerlies sweep the basin atmosphere clean. These episodes were subsequently used to analyse the transport and basin venting (de Foy et al., 2006c) using a mesoscale meteorological model and Lagrangian particle model. Whereas Elliott et al. (1997) suggested residence times as long as 2 days, this found residence times frequently as low as 6 to 12 h in the basin and little carry-over from day to day. The present analysis is based on the meteorological simulations described in de Foy et al. (2006c), making use of the 3 episode types and the short residence times.

1.2 Emission inventory

Emission inventories can be derived using either the "top-down" method, where total fuel and energy consumption are used for a whole region to determine surface emissions or the "bottom-up" method, where estimates of vehicle miles travelled and residential, industrial and commercial energy use patterns are considered. The 2002 official emission inventory for the MCMA used in this study was derived by the bottom-up method by the Comisión Ambiental Metropolitana (CAM) of the Mexican Federal District government (Comisión Ambiental Metropolitana, 2004). This contains annual totals for the criteria pollutants which need to be temporally and spatially distributed as well as speciated for VOCs (West et al., 2004).

Due to technology change, CO emissions have been decreasing despite increases in vehicular traffic. Schifter et al. (2005) develop a top-down estimate of vehicular emissions by combining fuel use statistics with emission factors obtained from in-situ remote sensing experiments. This suggests that, if anything, the official inventory may overestimate CO emissions. Jiang et al. (2005) obtain emission factors for the MCMA vehicle fleet by analysing data from the Aerodyne mobile laboratory (Kolb et al., 2004) for CO, black carbon, polycyclic aromatic hydrocarbons and other pollutants. For CO, a similar conclusion to Schifter et al. (2005) is drawn, that official inventory estimates are high but in general agreement. Zavala et al. (2006) analyse chase and fleet average mode data in detail, determining emission factors from individual vehicle plumes and obtaining emission estimates for individual vehicle types. This provides valuable information on NO_x, aldehydes, ammonia and certain VOC's which will be used to further refine the emission inventory and guide policy work. West et al. (2004) modelled the photochemistry in the basin during the IMADA campaign using the 1998 official inventory of the CAM, suggesting that emissions of CO need to be scaled by a factor of 2 and that of volatile organic compounds (VOCs) by a factor of 3.

Olivier and Berdowski (2001) develop the EDGAR global emission inventory at a 1 degree resolution. For Mexico the emissions of the MCMA are about ten times larger than anthropogenic sources outside of the basin. This means that within the accuracy of the present modelling work, regional emissions can be represented through appropriate settings of the boundary conditions.

On the regional scale, Kuhns et al. (2005) report on the development of an emission inventory for the northern part of Mexico as part of the BRAVO study. This includes the MCMA inventory but not the surrounding region. Also included are estimates of SO_2 emissions from the Popocatépetl volcano and the Tula industrial complex, two large point sources shown in Fig. 1. The Tula source consists of both a power plant and a refinery. The Popocatépetl volcano is an active volcano forming the southeastern edge of the MCMA basin. It has been under continuous monitoring by the Centro Nacional de Prevencíon de Desastres (CENAPRED). Kuhns et al. (2005) report SO_2 emission estimates made with a correlation spectrometer (COSPEC) as high as 18×10^6 tonne/year but more typically around 1.1 to 1.8×10^6 tonne/year.

Raga et al. (1999) analysed SO_2, CO and aerosol measurements in the MCMA and suggested that increased sulfate aerosol production in the city could be due to volcanic emissions. Jimenez et al. (2004) report on a field study carried

out between Popocatépetl and Puebla (to the east). Clear evidence was found of volcanic influence at the surface for 6 out of 17 days sampled.

Column measurements of CO can be used in conjunction with dispersion models to constrain emission inventories. For example, Yurganov et al. (2004) obtain CO columns from Fourier Transform Infrared (FTIR) spectrometers. A box model and the 3-D global GEOS-CHEM model (Bey et al., 2001) are used to evaluate the emissions from boreal wild fires in August 1998. Yurganov et al. (2005) extend the analysis to 2002 and 2003. Strong correlations are found between estimates from surface measurements and those from MOPITT CO columns.

1.3 Source identification

Blanchard (1999) reviews different methods for estimating the impacts of emission sources on air pollutant levels. These can be separated into data analysis methods and model-based methods. The latter includes forward and backward trajectory analyses as well as Eulerian dispersion models. Hopke (2003) reviews further developments of receptor models and back trajectory analyses. "Residence Time Analysis" and "Potential Source Contribution Function" are described and compared using case studies in the northeast of the U.S.

"Residence Time Analysis" was introduced by Ashbaugh et al. (1985). It is a 2-D gridded field that represents the probability that a randomly selected air parcel is to be found in a grid cell relative to the total time interval of the trajectory. Dividing the probability of a "dirty" air parcel being in a grid cell with the probability of any air parcel passing through that cell, one obtains the "Potential Source Contribution Function". This normalised field will have high values over regions of high emissions. The method was used to show that the dominant source of sulfur in the Grand Canyon national park was from southern California.

Sirois and Bottenheim (1995) define "Probability of Residence" by applying the Residence Time Analysis of Ashbaugh et al. (1985) to the trajectories associated with the highest and lowest 10% of air pollutant concentrations. A cluster analysis was then performed on all backward trajectories at the receptor site. Analysis of the pollution levels associated with each cluster showed agreement with the "Probability of Residence" method while providing additional information about air mass movements. Vasconcelos et al. (1996a) apply the method of Ashbaugh et al. (1985) to field campaign data in the Grand Canyon, again identifying southern California as the main source region. The spatial resolution of their results is analysed in Vasconcelos et al. (1996b). This suggested that the method has good resolution in source direction but significantly less in radial distance from the receptor site. Long trajectories (5 days in this case) have higher uncertainties, but short trajectories (3 days) can miss distant sources and suggest spurious source regions near the receptor.

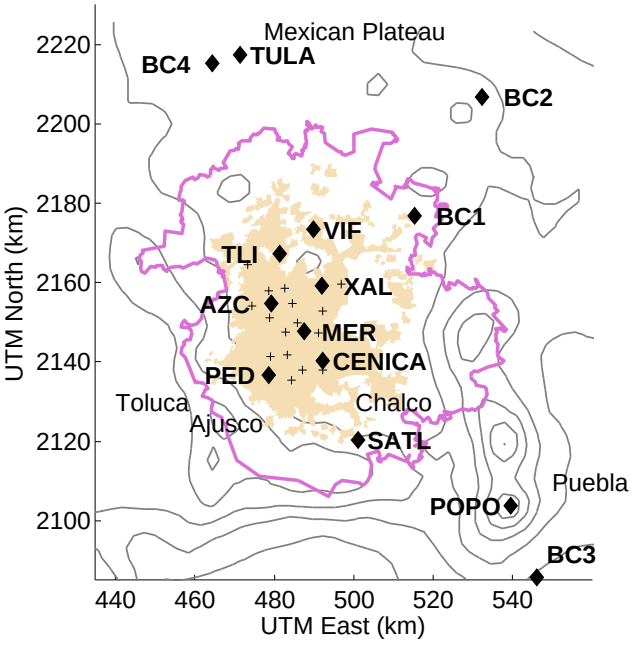

Fig. 1. Map of the MCMA showing the Tula industrial complex, Popocatépetl volcano, CENICA supersite, Santa Ana Tlacotenco (SATL) boundary site, SOF column measurement boundary sites and RAMA surface sites (crosses, see Fig. 11 for additional station names). Political border of the MCMA as of 2003 in pink, urban area in beige, terrain contour every 500 m.

Stohl (1998) reviews the applications and accuracy of trajectories. "Concentration Fields" are described as Residence Time Analysis multiplied by pollutant concentrations at the receptor site for each measurement time (Seibert et al., 1994). Lupu and Maenhaut (2002) show that the Potential Source Contribution Function and Concentration Field methods are in agreement over the identification of European emissions based on measurements at different peripheral sites. The bootstrap technique is used to estimate the statistical significance of potential sources, and known emission sources are shown to be correctly identified.

Use of single trajectories does not account for the spread in possible source directions due to vertical and horizontal mixing. Jiang et al. (2003) calculate retro-plumes by running a dispersion model, CALPUFF, in reverse mode. This yields the equivalent of Concentration Fields that account for all the processes parameterised in CALPUFF, including dispersion and deposition. By replacing single trajectory analyses with a Lagrangian particle dispersion model, Stohl et al. (2002) account for both physical dispersion and numerical uncertainty in the trajectory locations.

1.4 Vertical dispersion

As the resolution of meteorological models increases both in the horizontal and in the vertical, the parameterisation of the

surface energy budget and that of the vertical mixing become more important in terms of simulation accuracy (Zhong and Fast, 2003). Nevertheless, Berg and Zhong (2005) found that despite the different boundary layer schemes in MM5 and the different levels of mixing they simulate, there is little gain in the overall accuracy of the forecasts due to their increased complexity. Air quality models usually include a choice of vertical dispersion schemes based on output from the meteorological models, for example the widely-used parameterisation scheme of O'Brien (1970).

Evaluating vertical diffusion coefficients is difficult because the numerical representation does not account for the complexity of the physical process and because the diffusion coefficients cannot be measured directly. Atmospheric concentrations of radio-nucleides provides an indirect method of evaluating the dispersion. Vertical profiles of ^{222}Rn in the lower atmosphere have been used (Lee and Larsen, 1997), (Olivie et al., 2004).

For air quality models, the vertical dispersion has a direct impact on simulated surface concentrations. Nowacki et al. (1996) found excessive vertical mixing in the day time unstable boundary layer leading to errors in surface concentrations. Improvements in the specification of the vertical diffusion coefficients were suggested but evaluation was limited due to the lack of measurements of the vertical concentration profiles. Biswas and Rao (2001) report substantial differences between different models adding to uncertainties in ozone simulations and Roelofs et al. (2003) suggest that coarse vertical resolution may lead to excessive dispersion.

Brandt et al. (1998) analysed different vertical dispersion schemes and found that the simplest scheme of high vertical dispersion yielded the best results, suggesting that non-local dispersion is an important factor. Ulke and Andrade (2001) propose a new parameterisation which yields higher surface concentrations in the CIT model. They also highlight the problem of validating emissions inventories with surface data but no vertical profiles. Perez-Roa et al. (2006) use artificial neural networks to develop site-specific optimal estimates of vertical diffusion coefficients. They show improved surface concentrations of CO and particulate matter using the CAMx model, as well as possible adjustments to the emission inventory.

Jazcilevich et al. (2005) use vertical diffusion coefficients from the Burk-Thompson scheme in MM5 for their simulations of the MCMA. In contrast to West et al. (2004) who used the CIT coefficients, no adjustments factors are needed to the CO emission inventory. Although the 1994 official inventory is used rather than the 1998 one, this suggests that differences between models can impact the conclusions drawn about the inventory.

1.5 Outline

This paper makes use of Concentration Fields from backward trajectories and forward Eulerian dispersion modelling to analyse the emission inventory for CO and SO_2. Column measurements of CO are used as a constraint on the vertical dispersion scheme. SO_2 emission fluxes are estimated from large point sources so as to simulate their impact on the MCMA. Section 2 describes the models used and Sect. 3 the observations. The analysis of the emission inventory is split by pollutant: Sect. 4 looks at CO and Sect. 5 looks at SO_2. Each section is split into a first part using backward trajectories, a second part using Eulerian modelling and a discussion section.

2 Model description

The Pennsylvania State University/National Center for Atmospheric Research Mesoscale Model (MM5, Grell et al., 1995) version 3.7.2 was used to generate the wind fields as described in de Foy et al. (2006b). This uses three nested grids with one-way nesting at resolutions of 36, 12 and 3 km, with 40×50, 55×64 and 61×61 grid cells for domains 1, 2 and 3, respectively, and are the same simulations used in de Foy et al. (2006a). The initial and boundary conditions were taken from the Global Forecast System (GFS) at a 3-h resolution. High resolution satellite remote sensing is used to initialise the land surface parameters for the NOAH land surface model, as described in de Foy et al. (2006b).

The emission inventory used for CO and SO_2 is based on West et al. (2004) with updated totals from Comisión Ambiental Metropolitana (2004). The spatial pattern of the CO area sources is shown in Fig. 2a, and the point sources in Fig. 2c. The SO_2 emissions are shown in Figs. 2b and d. The temporal profile of both CO and SO_2 is shown in Fig. 3. This shows that the point sources are negligible for CO and small for SO_2, although including the Tula industrial complex and Popocatépetl volcano would change this picture. There is a clear peak at the morning rush hour, sustained traffic throughout the day and reduced emissions at night.

Stochastic particle trajectories are calculated using FLEXPART (Stohl et al., 2005), as described in de Foy et al. (2006c). Backward trajectories are calculated for specific fixed sites. For these cases, 100 particles per hour are released between 0 and 50 m above ground and are traced back for 48 h. Forward trajectories are calculated with the CO spatial and temporal distribution described above to provide simulated CO fields.

Residence Time Analysis was carried out using the particle simulations following Ashbaugh et al. (1985). For a one hour release, all particle positions at every hour of the simulation are stored. A surface grid is applied over the simulation domain, and all particle positions in each grid cell are totalled for the entire simulation. This gives "Residence Times", the grid corresponds to a time exposure photograph of the particle tracks, with values equivalent to the length of time spent in each cell by particles emitted.

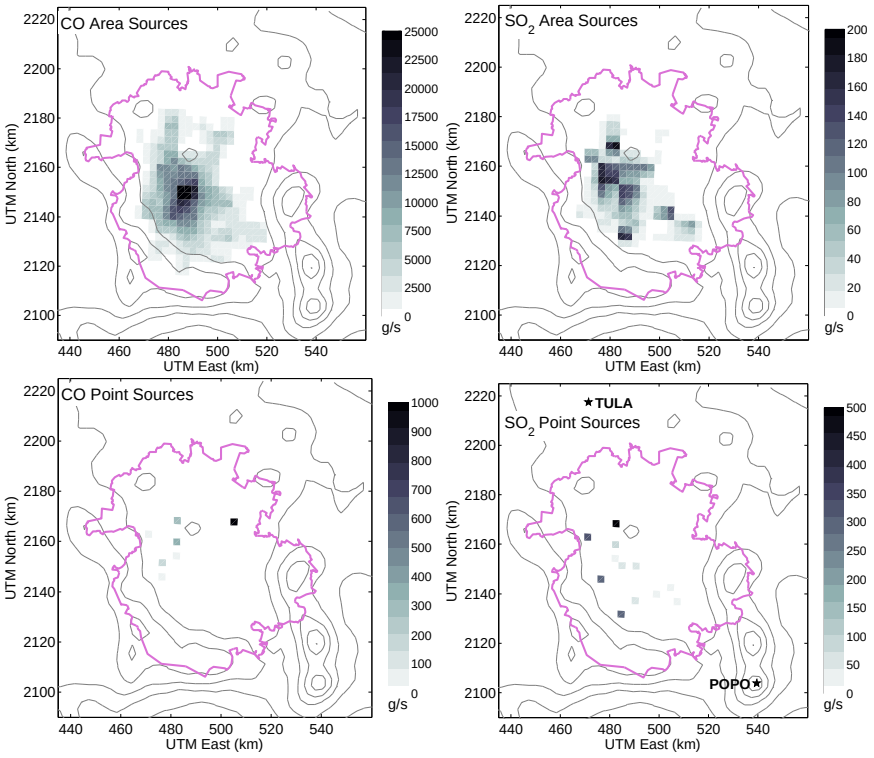

Fig. 2. Daily emission totals for CO (left) and SO_2 (right) from area (top) and point sources (bottom). Point sources are summed to the same grid as the area sources for ease of comparison. Note different scale for each plot. Location of Tula and Popocatépetl shown by the star (not colour coded).

The Residence Times can be summed for hourly releases during the whole campaign to identify preferred transport directions. In order to identify possible source regions, Concentration Fields were calculated. To derive these, Residence Times from backward trajectories are summed after scaling by the surface concentration at the release site for the corresponding hour, following Seibert et al. (1994). All the grids of particle paths passing over source regions will therefore be scaled up while clean air trajectories will be scaled to zero so that the final sum will reveal potential source regions. It should be noted however that this method is not able to distinguish between different points along the release path. As a result, the sensitivity of the method is much greater in terms of direction than in terms of distance from the source. Redistribution of Concentration Fields (Stohl, 1996) was tested for this test case but was not able to converge on a solution and was therefore not used. This was probably because the sources are too spread out and the receptor sites to close to the urban area.

Eulerian pollutant transport was calculated using the Comprehensive Air-quality Model with eXtensions (CAMx, ENVIRON, 2005), version 4.20. This was run on the finest MM5 domain at 3 km resolution with the first 15 of the 23 vertical levels used in MM5. This corresponds to approximately 5200 m above ground and 440 hPa over Mexico City. Chemistry was turned off and the simulation was carried out for just CO and SO_2 acting as passive tracers.

Vertical dispersion is treated with parameterisations based on surface and boundary layer parameters. These were obtained from MM5 which was run with the MRF boundary layer scheme (Hong and Pan, 1996). The coefficients of O'Brien (1970) (OB70) and of the CMAQ model (Byun, 1999) were tested in CAMx, but not those based on turbulent kinetic energy as this is not calculated by the MRF scheme.

CAMx version 4.20 had a number of improvements. Of particular relevance was the reduction in the horizontal diffusion and the time interpolation of the vertical diffusion coefficient. The first change lead to reduced mixing, but the second lead to increased mixing in the morning hours. While these compensated each other to some degree, the earlier mixing improved the concentration profiles during rush-hour.

3 Measurements

3.1 FTIR

Mobile column measurements of CO were made using Fourier Transform Infrared Spectroscopy (FTIR). A medium resolution spectrometer ($0.5\,cm^{-1}$) was used with a new 360-degree solar tracker. This system was used to evaluate

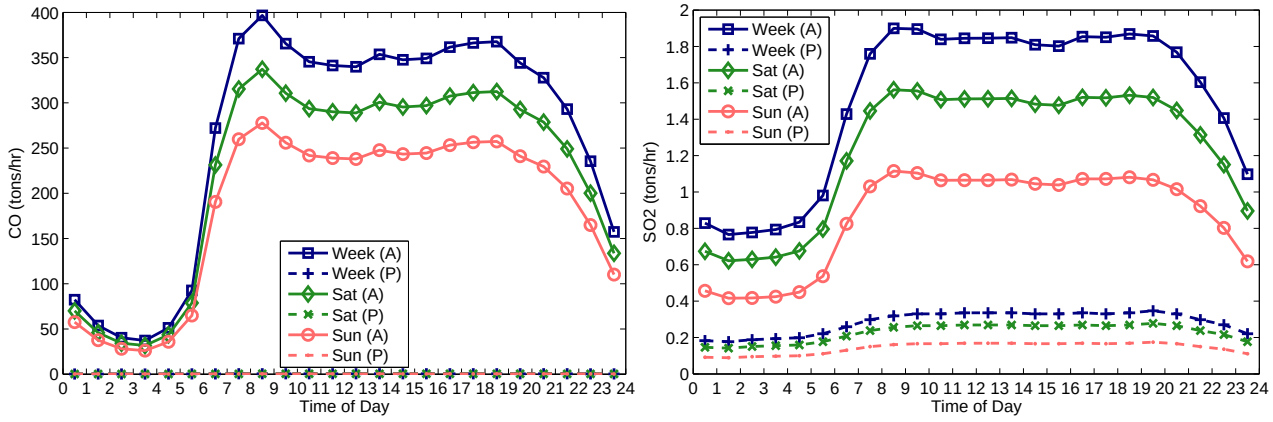

Fig. 3. Diurnal emission profiles for CO and SO_2 from area (A) and point (P) sources summed over the entire simulation domain for weekdays and week-end days. Tula industrial complex and Popocatépetl not included.

a number of species both in fixed site mode and in mobile mode to evaluate point source emissions with the Solar Occultation Flux method (SOF). This study makes use of the 126 total CO columns measured between 11 April and 1 May. Between 1 and 10 spectra are used for each measurement. By considering their standard deviation, the 95% confidence interval of the measurements is estimated to be 5%.

The long-path FTIR (LP-FTIR) system at CENICA consisted of a medium resolution ($1\,cm^{-1}$) spectrometer (Bomem MB104) coupled to a custom fabricated transmitting and receiving telescope. At the other side of the light path, a cubecorner array was mounted at a tower, making up a total folded path of 860 m (parallel to DOAS-1 described below). The system provided data with 5-min integration time continuously from 22:20 on 9 March to 00:00 on 29 April, except for a 12 h gap on 11 April. Spectra were analyzed using the latest HITRAN database cross sections (Rothman et al., 2003) and a nonlinear fitting algorithm. Data are available for the following species: CO, CO_2, HCHO, CH_4, N_2O and alkanes.

Separate long-path FTIR measurements were made at La Merced (MER) as described in Grutter et al. (2005) and Grutter (2003). A Nicolet interferometer was used with a ZnSe beamsplitter operating at $0.5\,cm^{-1}$ resolution. The liquid-nitrogen-cooled MCT detector had a working range of 600 to $4000\,cm^{-1}$. The equipment was mounted on top of two 4-storey buildings leading to a single path length of 426 m that was 20 m above ground level. Continuous data were available from 1 April to 4 May inclusive for 75% of the time. As for the CENICA FTIR, the spectra were analyzed with the HITRAN cross sections of Rothman et al. (2003). Data for the following species are available: H_2O, CO_2, CO, CH_4, C_2H_2, C_2H_4, O_3, NO, N_2O, NH_3, HNO_3 and HCHO. Uncertainties in the measurements are estimated to be within 5% but may be below 1% for the peaks.

3.2 Zenith sky UV/Visible spectroscopy

Remote sensing of SO_2 can be used to estimate emission rates. Whereas CO sources are spread out and CO plumes broad, SO_2 sources are more likely to be large point sources with individual well-defined plumes. Galle et al. (2002) developed a miniaturised ultraviolet sprectrometer to evaluate volcanic emissions. The "Mini-DOAS" is used to quantify emissions from 2 volcanoes and is compared with measurements from COSPEC. Elias et al. (2006) report further validation against COSPEC with agreement between the different systems within 10%. McGonigle et al. (2004) use the same technique for estimating power plant emissions of both SO_2 and NO_2. Emission rates of 5.2 kg/s of SO_2 were remarkably close to in-stack monitor values of 5.3 kg/s, suggesting that this method provides an accurate, low-cost, easily deployable means of estimating and validating large point sources in emission inventories.

The mini-DOAS system deployed used an Ocean Optics spectrometer with operating range of 280 to 390 nm and 0.6 nm resolution using the DOASIS (Kraus, 2001) and WinDoas (Fayt and van Roozendael, 2001) retrieval software. In mobile mode, columns of SO_2 are obtained along plume traverses. Multiplying the column integrated over the traverse by the average wind speed yields the emission estimates. Wind speed was measured at the ground. In addition, by looking at the time shift between the measurements along two different paths using a dual beam mini-DOAS it is possible to estimate the plume speed given an estimated plume height (Galle et al., 2006). The techniques yielded estimated speeds ranging from 3.4 m/s to 7.7 m/s for different traverses.

Six traverses were carried out for the Tula industrial complex on 1 May. This yielded an average estimated emission rate of 4.4 kg/s of SO_2. The standard deviation was 1.86 kg/s suggesting a 35% uncertainty in the measurements at 95% confidence interval.

On the afternoons of 27 and 28 April, two traverses of the plume of the Popocatépetl volcano yielded estimates of 11.1 and 8 kg/s. Daily summaries of volcanic activity are available from CENAPRED (http://www.cenapred.unam.mx/). These report between 2 and 25 low intensity exhalations of steam and gas everyday of the campaign. There were occurrences of small to moderate explosions on 17 April, on 24 to 25 April and on 27 to 28 April. The last episode involved the ejection of incandescent debris to a distance of about 800 m at night and some moderate amplitude tremors. In addition to exhalations and explosions, the volcano is a passively degassing eruptive volcano with continuous SO_2 emissions in the absence of any visible eruptions (Delgado-Granados et al., 2001).

3.3 DOAS

The DOAS technique has been described in Platt (1994). Two long-path DOAS (LP-DOAS) systems were mounted at CENICA. SO_2 was measured by detection of the unique specific narrow-band (5 nm) absorption structures in the ultraviolet spectral range (near 300 nm). Both LP-DOAS were installed on the rooftop of the CENICA building, from where light of a broadband UV/vis lightsource (Xe-short arc lamp) was projected into different directions into the open atmosphere: DOAS-1 pointed towards an array of retro reflectors located in southeasterly direction (TELCEL tower), DOAS-2 pointed towards an array of retro reflectors located in southwesterly direction on top of the local hill Cerro de la Estrella. The lightbeam was folded back into each instrument and spectra were recorded using a Czerny-Turner type spectrometer coupled to a 1024-element PDA detector. The average height of the light path was 16 m and 70 m above ground, the total path length was 860 m and 4.42 km, the mean SO_2 detection limits were 0.26 ppbv and 0.15 ppbv, respectively. SO_2 reference spectra were recorded by introducing a quartz cell filled with SO_2 into a DOAS lightbeam. Spectra were analysed using nonlinear least squares fitting routines by Fayt and van Roozendael (2001) and Stutz and Platt (1996). Reported concentrations are based on the absorption cross section of Vandaele et al. (1994). Data were available for DOAS-1 from 06:00 on 3 April until 11:00 on 2 May and for DOAS-2 from 00:00 on 3 April to 17:45 on 11 April and from 08:40 on 18 April to 13:30 on 3 May. Other data from DOAS-1 and DOAS-2 are described in Volkamer et al. (2005b) and Volkamer et al. (2005a). Uncertainties in the data are estimated at 5%. At MER, a commercial DOAS system (Opsis) was installed with the same open-path as the FTIR (Grutter et al., 2005) providing data at 5-min resolution from 1 April to 4 May.

3.4 Monitoring stations

The MCMA-2003 field campaign was based at the National Center for Environmental Research and Training (Centro Nacional de Investigación y Capacitación Ambiental, CENICA) super-site. Figure 1 shows the location of the measurement sites used in this study. A monitoring site measuring meteorological parameters and criteria pollutants is under continuous operation there. In addition, the CENICA mobile van with similar equipment was deployed within the grounds of a primary school in Santa Ana Tlacotenco (SATL). This is a small village on the southeastern edge of the basin overlooking the MCMA. Surface criteria pollutant concentrations are measured throughout the city by the Ambient Air Monitoring Network (Red Automática de Monitoreo Atmosférico, RAMA). These data were available both at the raw 1-min resolution and in 1-h averages.

Detailed information on all the stations is available online (http://www.sma.df.gob.mx/simat/, see "Mapoteca") including descriptions and photographs of the surrounding areas. Chow et al. (2002) contains a table with information on many of the sites in this study (note that G17 = IMP, G12 = UIZ, G05 is close to SAG). The reader is referred to these sources for information supporting the discussion of individual stations.

CO measurements were made using the Teledyne API model 300 CO analyser which uses the gas filter correlation method. Infrared radiation at 4.7 µm passes through a rotating gas filter wheel at 30 Hz. This cycles between the measurement cell containing nitrogen which does not affect the beam before passing through the detection cell, and the reference cell containing a mixture of nitrogen and CO which saturates the beam. Measurement accuracy is estimated to be below 5% although overall accuracy including site location and sampling issues is below 15%.

SO_2 measurements were made using pulsed UV fluorescence (Teledyne API models 100 and 100A). UV radiation of 214 nm is passed through the detection cell and the photomultiplier tube is fitted with a filter in the range of 220 to 240 nm. The CENICA data had a baseline offset of 3 ppb which was substracted from the data. The measurements were digitised with 1 ppb increments, and had a stated instrument accuracy of 1% but likely overall measurement accuracy below 15%.

The timezone in the MCMA was Central Standard Time (CST=UTC–6) before 6 April and daylight saving time (CDT=UTC–5) thereafter. The field campaign policy specified the use of local time for data storage and analysis, a convention that will be followed here with times in CDT unless marked otherwise.

4 Carbon monoxide

Carbon monoxide is emitted mainly by mobile sources and acts as a passive tracer on the time scales of the MCMA. It is therefore a useful quantity to verify the simulated transport by both Lagrangian and Eulerian models. For Lagrangian simulations, Concentration Field analysis can be used to

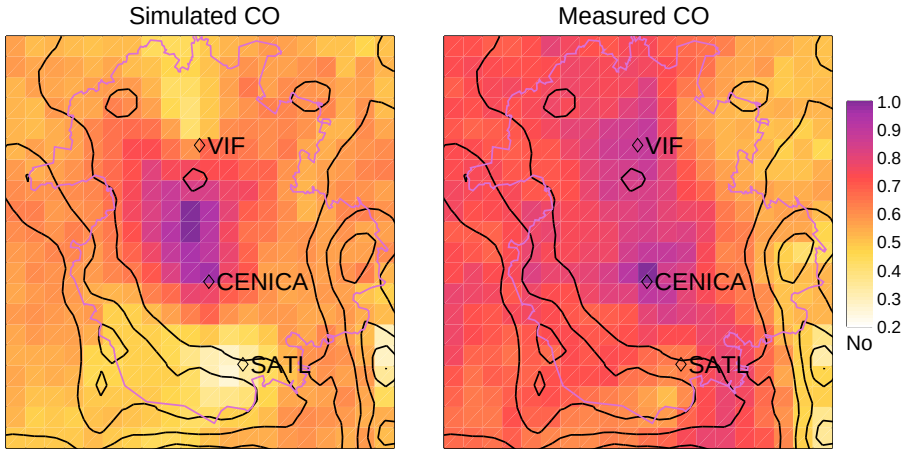

Fig. 4. Concentration Field analysis of CO using simulated (left) and measured (right) time series of concentrations at CENICA, VIF and SATL based on back-trajectories every 2 h at each location. High non-dimensional number (purple) indicates possible source regions, low numbers (white) indicate areas with low emissions.

identify possible source regions which can then be compared with known inventories. For Eulerian models, comparisons with surface measurements are used to verify model performance. Column measurements are used to verify the total emissions and to identify potential adjustment factors.

4.1 Concentration field analysis

Concentration field analysis was applied to CO concentrations at three locations: CENICA near the centre of the city, VIF to the north of the MCMA and SATL to the south. In order to increase the sensitivity of the method in the radial distance from the source, it can be applied to multiple stations at once. Because the sources of CO are better known than SO_2, CO concentrations can be used to validate concentration field analysis before using it to identify unknown sources of SO_2. As a first test of the sensitivity of the method, it is first applied to simulated concentrations obtained from forward runs of the model. In this way, meteorological uncertainties are removed. Ideally, we would recover the initial emission inventory. Results are shown in Fig. 4. Comparison with the spatial emission map in Fig. 2 shows that the method is able to recover the urban core of the emissions. As expected, there is a high background as the method cannot distinguish distances from the observation sites. Note that this problem is reduced around VIF and SATL, and would be further reduced by adding stations all around the MCMA.

Concentration field analysis using measured concentrations and simulated trajectories is shown in Fig. 4. The method is still able to identify the urban emission in the centre, but the picture is much less focused. There are small but noticeable impacts from wind flows from the Mexican Plateau to the north, from the pass from Toluca to the west and from the Chalco passage in the southeast. At this point, it is not possible to say if this is due to limitations in the wind simulations, or if it is evidence of impacts from neighbouring airsheds. To further test the method, individual Concentration Fields were calculated for VIF and SATL (not shown). While these are on opposite sides of the MCMA, the method correctly identifies the urban area as the CO source suggesting that the results are not an artefact of prevailing winds.

4.2 Eulerian modelling

CAMx simulations from three test cases will be presented. Case 1 was with the OB70 vertical diffusion coefficient and case 2 with the CMAQ coefficients. Case 3 was similar to case 2 with emissions of CO scaled by a factor of 2. The minimum vertical diffusion coefficient was set to $1\,m^2/s$ for CMAQ. For OB70, the domain wide minimum was set to $0.1\,m^2/s$ and the kvpatch processor was used to reset the minimum in the bottom 500 m layer to $1\,m^2/s$ over urban areas and $0.5\,m^2/s$ over forests. Simulations were initialised on 31 March 2003 and run for 35 days. Emissions were scaled depending on the type of day. Saturday and Sundays had emissions that were 15% and 30% lower than weekdays. In addition, school vacation days (13 to 25 April 2003 inclusive) were reduced by 10%, Good Friday (18 April) was reduced by 50% and Maundy Thursday (17 April) was reduced by 30%. Initial fields of CO were set to 0.25 ppm at the surface decreasing to 0.125 ppm at the domain top. These values were obtained from inspection of boundary site data as well as simulation results from the GEOS-CHEM model (Bey et al., 2001).

Profiles of vertical diffusion coefficients are shown in Fig. 5 for both the OB70 and CMAQ algorithms. At night, the values correspond to the specified minimum value except for a shallow layer below 500 m with some mixing. The surface CMAQ coefficients are larger, but the surface layer is shallower than for OB70 and the values rapidly drop to

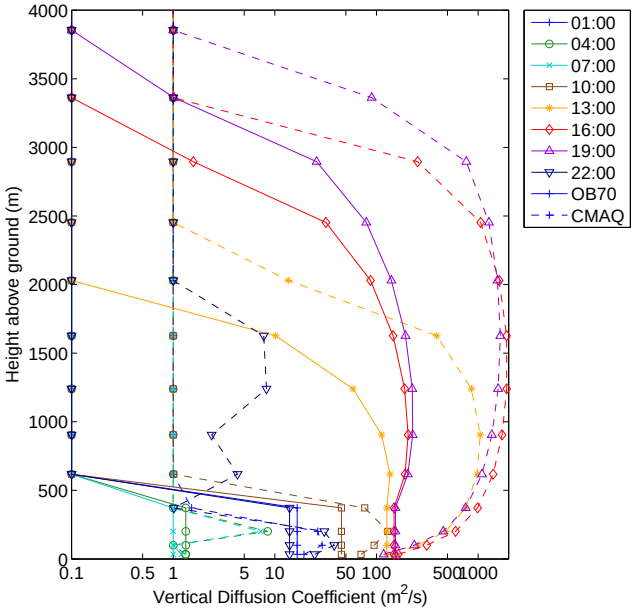

Fig. 5. Comparison of vertical diffusion coefficients at MER from the OB70 (−) and CMAQ (−−) algorithms by time of day for 15 April 2003. Values obtained from the CAMx pre-processor for MM5 results using the MRF boundary layer scheme. See text for treatment of minimum value. Note the log scale.

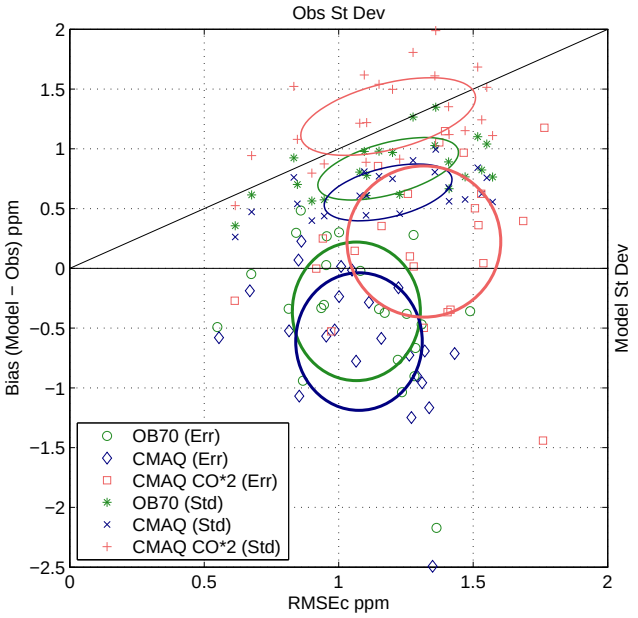

Fig. 6. Statistics diagram for surface CO for 3 cases for all stations with available data for the entire duration of the campaign. Each error point (Err) represents the bias versus the RMSEc (Standard deviation of errors) at a measurement station. Standard deviation points (Std) show the model standard deviation versus that of the measurements, which should be of similar magnitude.

the specified minimum value. During the day, the mixed layer develops rapidly with maximum mixing reached between 16:00 and 19:00. The CMAQ coefficients are substantially higher and, more importantly, extend farther upwards than OB70. By 22:00, mixing has returned to the night-time norm although CMAQ has residual mixing in a layer aloft.

The bias, centred root mean square error (RMSEc, also called standard deviation of errors) and Pearson correlation coefficient of the model simulations are shown in Table 1 for each RAMA CO monitor for the 34 day period from 1 April to 4 May 2003. Fig. 6 shows the model performance using the statistical diagram introduced in de Foy et al. (2006b). The bias is plotted versus the RMSEc for each station. The standard deviations of the simulations are plotted versus those of the measurements to provide context to the magnitude of the errors. In order to compare the simulations, ellipses are drawn with centres at the mean of the performance metrics and radii corresponding to the standard deviations of the metrics.

Ideally, bias and RMSEc should be close to 0 and standard deviations of the simulations should be equal to those of the model. Furthermore, RMSEc should be smaller than the standard deviations. From the table and figure, it can be seen that the negative bias of the CMAQ simulations is reduced with OB70 and that errors are also slightly decreased. Doubling the emission inventory causes a positive bias and increases the RMSEc to greater than the standard deviations of the concentrations.

Performance analysis of the meteorological simulations by episode type showed that the best simulations were obtained for the O3-South episodes and that simulations for the Cold Surge episodes were noticeably worse (de Foy et al., 2006a). As the same pattern is observable for CO simulations, the correlation coefficients for the OB70 simulations were separated into days with good performance and days with poor performance, see Table 1. The 15 “Good CO” days were 13 to 16 April and 23 April to 4 May excluding 27 April. This includes both O3-South events and the second, and longest, O3-North event. The remaining 19 “Bad CO” days include the three Cold Surge episodes as well as the first O3-North episode which was the one that followed a period of heavy rains. The difference in correlation coefficients can be clearly seen. From this point on, the analysis will focus on the “Good CO” days.

Table 1 shows considerable variation in the performance metrics at different stations. For example, MER and IMP are located in the city centre near high emissions but are on a school and campus-like environment respectively, shielding them from emissions in the immediate vicinity. Poor performance at PED, which is in a leafy suburb with low emissions, suggests that the spatial distribution of the emission inventory could be re-examined. Also poorly performing is TAX, in this case quite possibly because it is located near a major bus transport hub. Finally stations such as MIN and SAG have noticeably weaker performance than near-by

Table 1. Comparison statistics of surface CO concentrations for 3 model cases versus all RAMA measurements available. Statistics calculated for the 34 day period ("All Days") or for subsets ("Good CO" and "Bad CO"), see text.

RAMA Station	OB70 Bias All Days	RMSEc	r	r Good CO	r Bad CO	CMAQ Bias All Days	RMSEc	r	CMAQ CO*2 Bias All Days	RMSEc	r
ARA	−1.04	1.24	0.54	0.67	0.41	−1.25	1.27	0.52	−0.50	1.32	0.52
ATI	−0.05	0.67	0.46	0.52	0.37	−0.19	0.67	0.36	0.25	0.94	0.36
AZC	0.27	0.96	0.58	0.64	0.50	0.02	1.01	0.47	0.97	1.46	0.47
BJU	0.30	1.00	0.59	0.65	0.55	−0.02	1.05	0.50	1.05	1.37	0.50
CES	−0.31	0.95	0.51	0.51	0.59	−0.52	0.99	0.45	0.15	1.06	0.45
EAC	−0.77	1.22	0.50	0.57	0.44	−0.90	1.29	0.40	−0.37	1.41	0.40
HAN	−0.36	1.49	0.39	0.57	0.24	−0.71	1.43	0.39	0.40	1.69	0.39
IMP	−0.38	1.25	0.58	0.74	0.47	−0.73	1.26	0.55	0.36	1.52	0.55
LAG	0.28	1.28	0.55	0.61	0.50	−0.16	1.22	0.50	1.18	1.77	0.50
MER	−0.34	1.15	0.59	0.76	0.49	−0.78	1.06	0.57	0.50	1.51	0.57
MIN	−2.17	1.36	0.37	0.40	0.37	−2.49	1.35	0.31	−1.44	1.76	0.31
PED	0.30	0.84	0.42	0.43	0.40	0.07	0.85	0.31	0.86	1.15	0.31
PLA	0.03	0.95	0.52	0.63	0.45	−0.24	1.00	0.40	0.62	1.26	0.40
SAG	−0.94	0.87	0.43	0.50	0.38	−1.07	0.85	0.43	−0.53	0.97	0.43
SUR	−0.33	0.94	0.55	0.61	0.50	−0.57	0.95	0.51	0.35	1.16	0.50
TAC	0.48	0.86	0.53	0.57	0.45	0.23	0.86	0.42	1.15	1.40	0.42
TAX	−0.67	1.29	0.45	0.44	0.49	−0.96	1.31	0.38	0.04	1.54	0.38
TLA	−0.02	1.08	0.49	0.57	0.43	−0.28	1.11	0.38	0.62	1.53	0.38
TLI	−0.34	0.81	0.46	0.58	0.36	−0.52	0.82	0.42	−0.00	0.92	0.42
UIZ	−0.37	1.17	0.34	0.52	0.30	−0.59	1.16	0.33	0.10	1.26	0.33
VAL	−0.90	1.28	0.55	0.69	0.43	−1.17	1.34	0.50	−0.35	1.42	0.49
VIF	−0.49	0.55	0.47	0.57	0.41	−0.58	0.55	0.43	−0.27	0.61	0.43
XAL	−0.47	1.31	0.56	0.66	0.44	−0.69	1.32	0.59	0.02	1.28	0.59
Mean	−0.36	1.07	0.50	0.58	0.43	−0.61	1.08	0.44	0.22	1.32	0.44
St Dev.	0.58	0.24	0.07	0.09	0.08	0.58	0.24	0.08	0.63	0.29	0.08

stations MER and XAL, respectively. This can suggest impacts of neighbouring emissions or micro-meteorological effects. MIN for example is located inside an elevated roundabout (rotary/glorieta) with high traffic emissions very close to the monitor air-intake. Detailed comparison of the metrics with the station location and surroundings (see Sect. 3.4) in the future could point to possible weaknesses in both modelling and monitoring.

4.2.1 Column measurements

Comparisons of the statistical metrics for the 3 cases suggest that the OB70 scheme is better than the CMAQ scheme with or without adjustments in the emission inventory. These are entirely based on surface measurements however and do not account for the amound of CO in the atmosphere. A total column count of CO molecules can be used to evaluate the model simulations irrespective of their accuracy at the surface and hence to provide a constraint on the level of CO emissions.

Solar FTIR measurements of the CO columns are compared with simulated columns from the 3 model cases in Figures 7, 8 and 9. An offset of 0.52×10^{18} molecules/cm^2 was applied to the model columns to account for the CO above the domain top, corresponding to free tropospheric concentrations of 70 ppb above 440 hPa and 50 ppb above 120 hPa.

Agreement between model and observations is particularly good on 15 April. Unlike many urban areas where the columns increase throughout the day, CENICA experiences a steady reduction starting at noon. This is well captured by the model and is due to dilution caused by the gap flow (de Foy et al., 2006a). The small difference between the OB70 and CMAQ cases but the large difference with the CMAQ case with double CO emissions shows that the columns are sensitive to the emission levels and not the surface concentrations. The case with increased emissions clearly leads to excess CO in the atmosphere.

There was a sharp drop in emissions on 18 April which was Good Friday, a day when all schools and businesses are closed (de Foy et al., 2005). This can be seen in the measurements and is correctly captured by a 50% scaling factor in the model. The diurnal trend of the columns suggests that the diurnal profile of the emissions needs to be adjusted however. Agreement on 21 April is not nearly as good. This

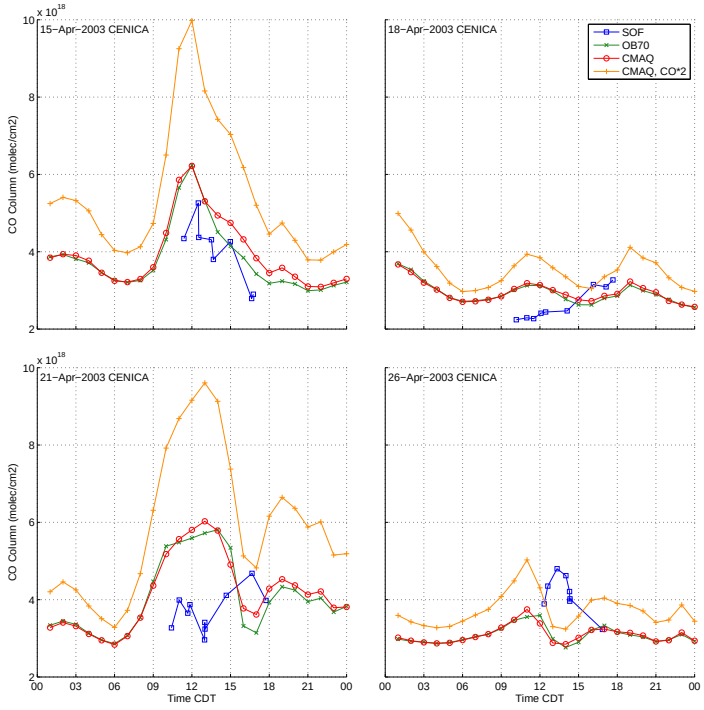

Fig. 7. Total column of CO measured by Solar Occultation Flux (SOF) versus model simulations for 3 simulation cases for different campaign days at CENICA.

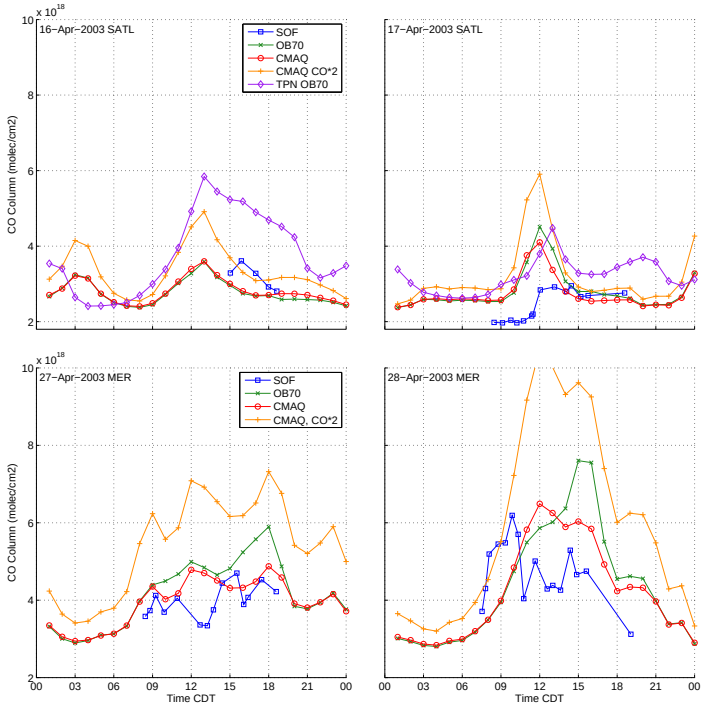

Fig. 8. Total column of CO measured by Solar Occultation Flux (SOF) versus model simulations for 3 simulation cases for different campaign days at Santa Ana (SATL) and La Merced (MER). TPN OB70 shows base case at Tlalpan, 20 km west of SATL, to highlight impact of gap flow.

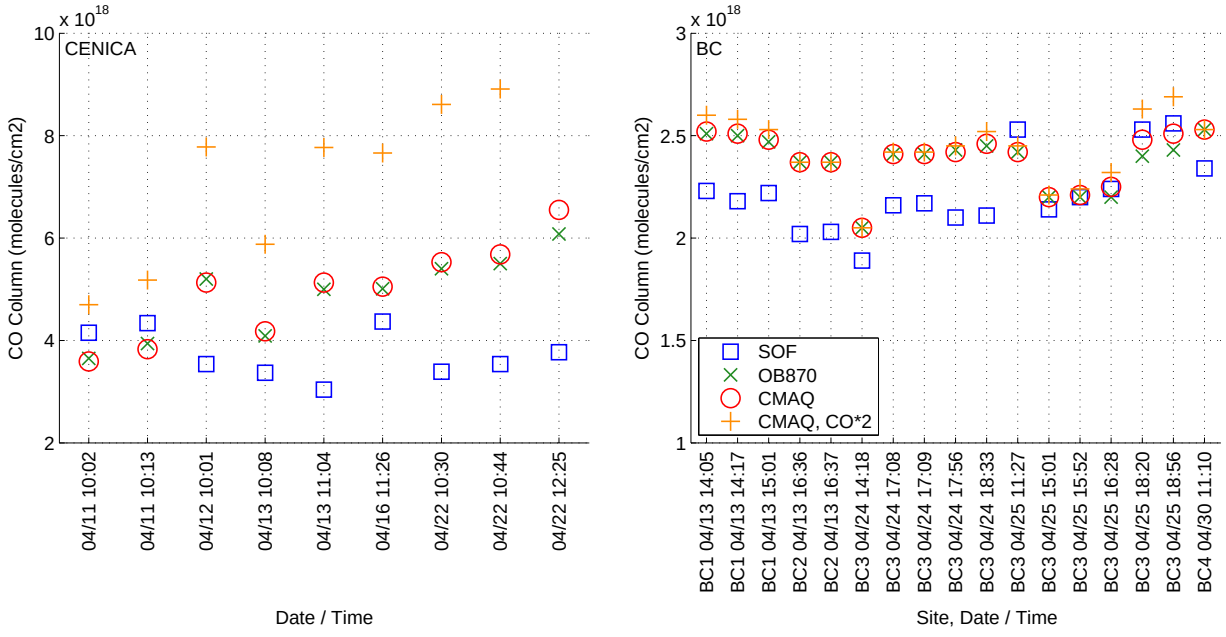

Fig. 9. Total column of CO measured by Solar Occultation Flux (SOF) versus model simulations for individual measurements at CENICA and at the boundary sites (see Fig. 1 for site locations).

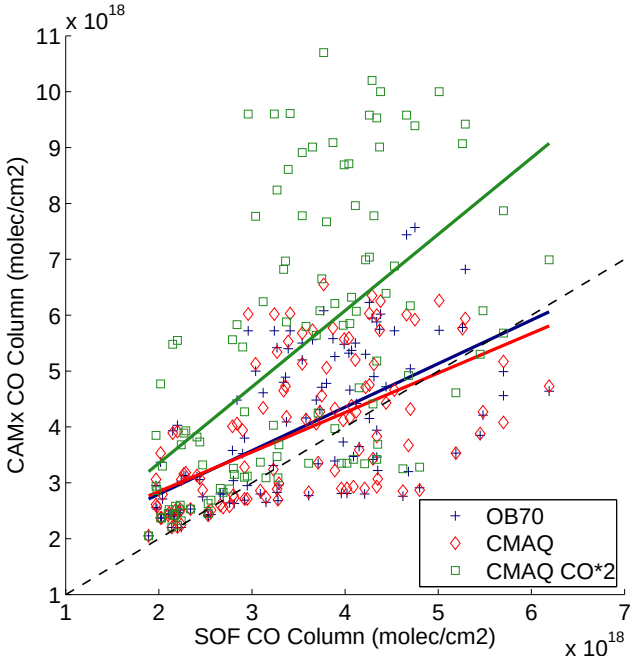

Fig. 10. Scatter plot of total column of CO measured by Solar Occultation Flux (SOF) versus model simulations for the 3 model cases. See Table 2 for coefficients of lines of best fit.

is attributable to the fact that this is a Cold Surge day with poorer model performance as described above.

At Santa Ana (SATL), on 16 April the columns show a slow decline after a 15:00 peak. On 17 April the afternoon decline is more gradual and follows a step increase at 12:00, when the urban plume reaches the southern basin rim. The trend is correctly captured on 16 April, but the simulated levels are too low. On 17 April, the levels are higher and the sharp increase occurs 2 hours earlier. Wind circulation at SATL are very sensitive to the strength and timing of the gap flow from the southeast (de Foy et al., 2006a). Columns 20 km to the west at TPN for the OB70 case show much higher levels on 16 April and somewhat higher levels on 17 April but a correct timing of the increase. This suggests that small changes in the gap flow can lead to large discrepancies in the model agreement.

Table 2. Least squares fit ($y=mx+c$) for correlation of SOF CO columns with 3 model simulations.

	OB70	CMAQ	CMAQ CO*2
m	0.78	0.71	1.37
95% bounds on m	0.58, 0.97	0.52, 0.90	0.99, 1.74
c ($\times 10^{18}$)	1.24	1.43	0.62
r	0.36	0.33	0.32

At La Merced (MER), especially on 27 April, the simulated columns of CO are at the right level without adjusting the emission inventory. The columns rise and fall under the competing impact of traffic and wind transport (Garcia et al., 2006).

Boundary conditions in the model were verified by comparing columns at boundary sites to the north of the MCMA

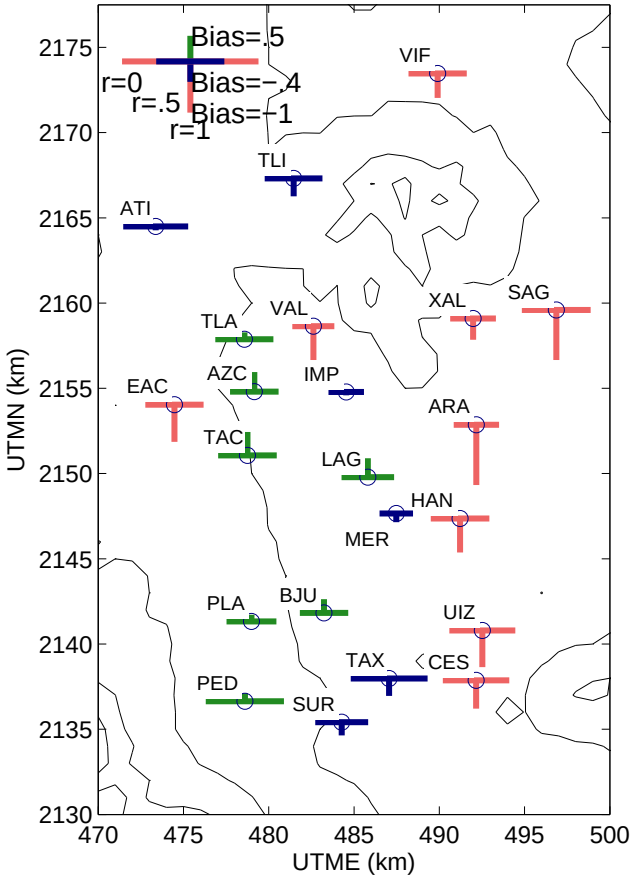

Fig. 11. Bias (vertical lines) and correlation coefficient (horizontal lines) CAMx OB70 vs. RAMA measurements for all stations except MIN, for "Good CO" days. Green for positive bias (model greater than observations), blue for negative bias smaller than 0.4 ppm and red for large negative bias. Correlation coefficient is plotted symetrically around the origin, short horizontal bars indicate good agreement.

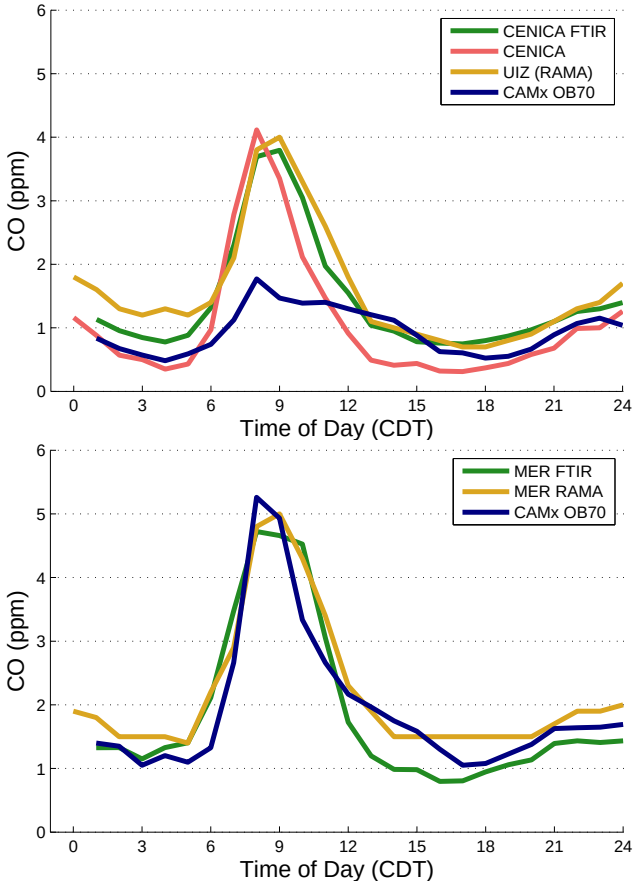

Fig. 12. Diurnal profiles of median concentrations of CO at MER and CENICA comparing monitoring data, FTIR data and CAMx results for "Good CO" days.

near Teotihuacan and Pachuca and outside the basin on the slopes of the Popocatépetl. The agreement was good, with values ranging from 2.0×10^{18} to 2.5×10^{18} molecules/cm^2.

Least squares fit of the simulations to the models are shown in Fig. 10 and Table 2 for the 3 cases along with 95% confidence bounds on the slope of the agreement. For the linear fit without constraining the y-intercept to 0, the uncertainty on the slopes are large and suggest that the base emission inventory could underestimate the actual CO levels. At 95% confidence level this would suggest that the method cannot distinguish between adjustment factors (a slope of 1 is within, or close to, the range for all 3 cases). If we constrain the y-intercept to 0 on the grounds that the boundary conditions are within 10% (0.25×10^{18} molecules/cm^2) of the true value (Fig. 9), then we obtain slopes in the range of 1.05 to 1.17 for OB70 and 1.42 to 1.64 for CMAQ with double CO. This provides stronger evidence that the current emission inventory is at the right level and that no adjustments are currently warranted.

4.2.2 Spatial analysis

Based on the analysis above, the case with unchanged emissions and OB70 vertical diffusion will be retained as the base case for further analysis. Figure 11 shows the bias and error for each station for the 15 days of the "Good CO" episodes. A clear pattern emerges, with positive bias (simulations higher than measurements) for central and southwestern stations and negative bias for northern and eastern stations. The correlation coefficient is highest (smaller bars) in the city centre and decreases in the periphery.

Median diurnal profiles of simulated and measured CO concentrations for CENICA and MER are shown in Fig. 12. At MER there is good agreement between the RAMA measurements, the FTIR and the model simulations. At CENICA, the early morning peak is clearly captured by all the measurements, but is not represented in the model. During the rest of the day, the FTIR measurements are higher than the CENICA data but comparable to the RAMA data. This discrepancy should be investigated, especially if the measurements are used to validate the emission inventory.

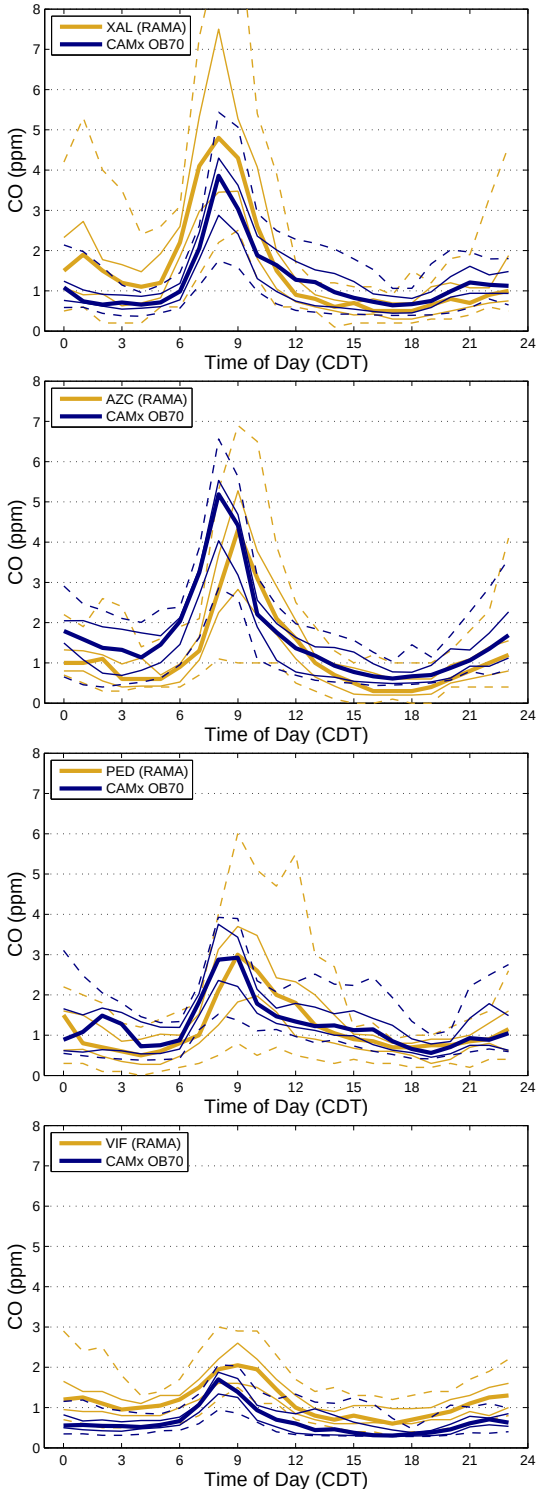

Fig. 13. Diurnal profiles of CO at selected RAMA stations for "Good CO" days. Bold line is the median, thin line the 25 and 75 percentile and dashed line the range. Measurements in yellow, model simulations in blue.

Further diurnal profiles for XAL, AZC, PED and VIF are shown in Fig. 13. At XAL, the pattern is well-captured but the predictions are too low. This is particularly acute in the morning with a delay in the rise of predicted concentrations. At PED, the opposite is true, with too high emissions in the early morning. VIF, to the north of the city, has much lower concentrations. Nonetheless, they are under-predicted by the model. At AZC, the morning peak starts too soon and rises too high, whereas at neighbouring VAL (not shown), the timing is correct but concentrations drop off much faster than the measurements. This illustrates the pitfalls of comparing gridded model results with point measurements and the need to consider carefully station location.

4.3 Discussion

The Concentration Field Analysis for CO shows that the method is able to correctly identify known sources based on surface data from the monitoring network. The method was shown to be robust with respect to station location and the prevailing wind directions. The analysis can be applied to individual stations first with model concentrations and then with actual measurements in order to identify the upwind regions that affect a monitor and wether the measurements are dominated by local or more regional transport.

Column measurements of CO were shown to provide a necessary constraint in evaluating potential adjustment factors to the emission inventory. Uncertainty in the model simulations based on statistical metrics and data comparisons can be estimated to be between 35% and 50%. The high errors in the model have been attributed to complex meteorology in the basin (de Foy et al., 2006a). While this precludes a definite conclusion on the adjustment factors for CO emissions, it nonetheless suggests that current levels are consistent with concentrations.

Spatial patterns of Eulerian model performance can be used to evaluate the spatial distribution of the inventory. Positive bias in the southwest and negative bias to the east and north are consistent with current patterns of urbanisation. This suggests possible adjustments in terms of city sectors, although it is too crude to resolve features on the scale of individual grid cells. The effect can be clearly seen at CENICA. In the simulations, the station is on the edge of the city edge and does not see the strong morning rush hour peak in measured CO.

Comparisons of diurnal profiles at individual stations can be used to evaluate the temporal distribution of the emissions and to suggest modifications by time of day. Varying emissions during vacations and holidays are a source of uncertainty and model under-performance that has not been quantified in the present study. Scaling factors for high and low emission days were deduced from morning CO observations. Traffic data will be needed to refine these as the biggest change in emissions by day of week and type of day may be

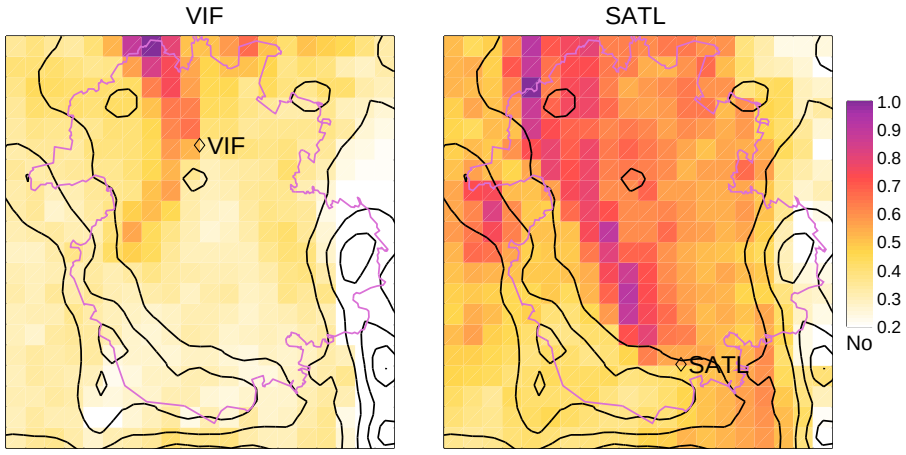

Fig. 14. Concentration Field analysis of SO_2 based on measured concentrations and simulated back-trajectories at VIF (left) and SATL (right) showing possible northwest source region.

the temporal and spatial distribution rather than the overall emission level.

5 Sulfur dioxide

5.1 Concentration field analysis

Concentration field analysis was performed for SO_2 in the same way as for CO, see Sect. 4. Results for VIF and SATL, the stations most to the north and south respectively, are shown in Fig. 14. Both of these point to a focused source to the northwest of the city. The signal at VIF is particularly clear, with only small contributions from areas southwest of the station. Because SATL is further away and on the southern edge of the basin rim, the picture is more diffuse. The trace from the northwest is still clearly visible however, with suggested transport southwards along the western edge of the basin.

5.2 Eulerian modelling

CAMx simulations of SO_2 were carried out with the OB70 vertical diffusion scheme. In addition to the point and area sources from the emissions inventory, point sources for the Tula industrial complex and for the Popocatépetl volcano were added as described in Sect. 3. Generic stack parameters were used which do not affect the long range transport of the plume. Emissions were set to 5 kg/s for Tula and 10 kg/s for Popocatépetl based on the mini-DOAS estimates. The emissions were held constant in time. These emissions correspond to 158×10^3 tonne/year and 316×10^3 tonne/year respectively. All boundary and initial conditions for SO_2 were set to 1 ppb based on GOME satellite retrievals available at the Belgian Institute for Space Aeronomy (IASB-BIRA).

Figure 15 shows time series of SO_2 at VIF to the north of the city and CENICA to the southeast for measurements and simulations that include the Tula and Popo point sources. The shading in the background indicates the fraction of the simulated SO_2 due to the Tula industrial complex and the volcano obtained by running separate tracer simulations. This shows that the model would not simulate the sharp peaks if emissions from Tula were not included. At VIF,

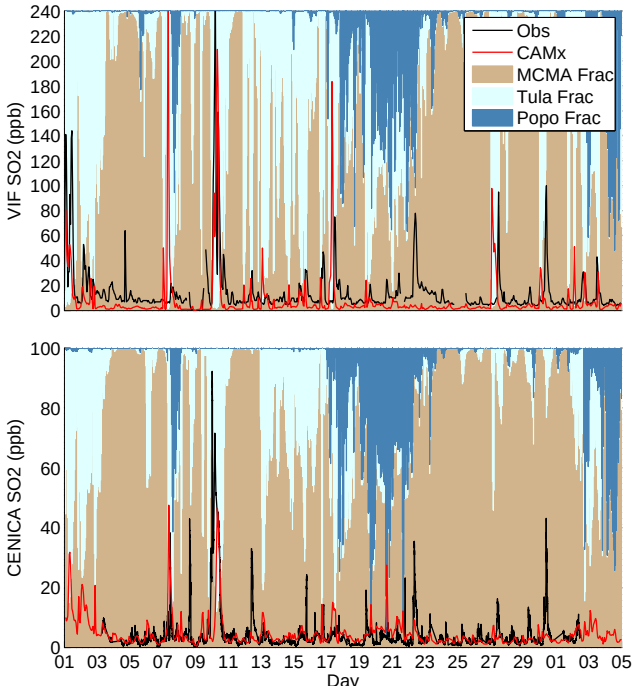

Fig. 15. SO_2 time series at VIF and CENICA showing measured (black) versus modelled (red) concentrations for the entire campaign. Coloured shading indicates the fraction of simulated SO_2 that is due to different sources (MCMA, Tula and Popocatépetl).

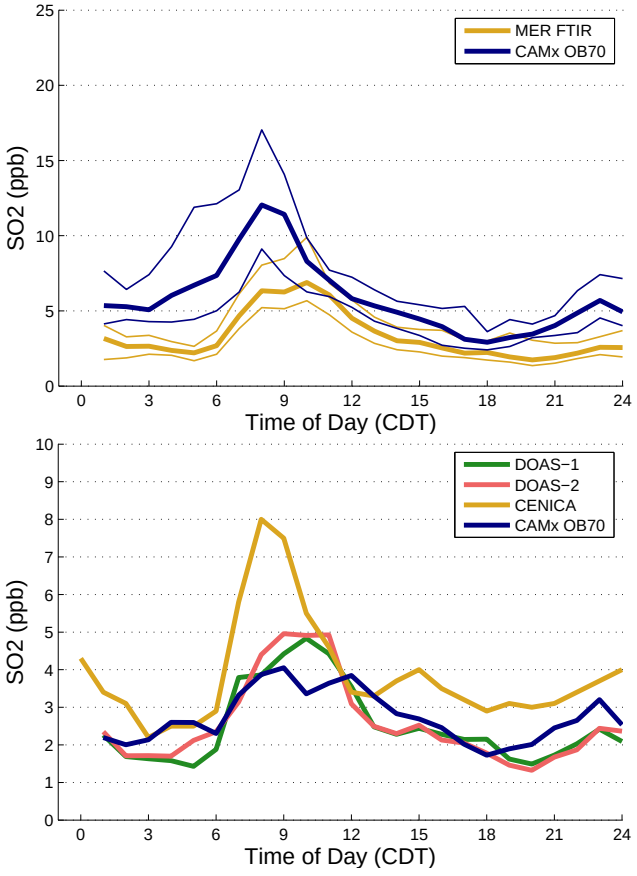

Fig. 16. Diurnal profiles of SO_2 at MER and CENICA comparing monitoring data, DOAS data and model results for "Good CO" days. Bold line is the median, thin line the 25 and 75 percentile.

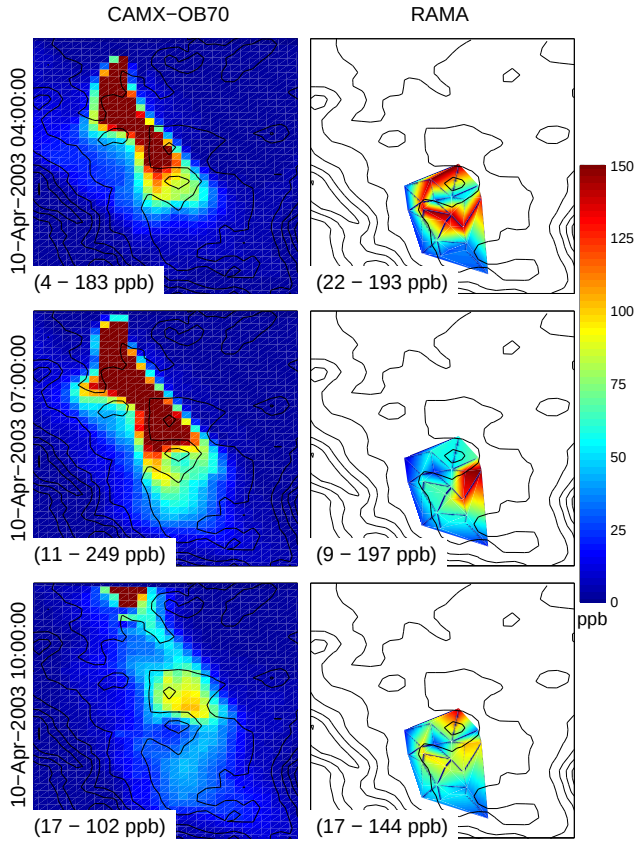

Fig. 17. Surface concentration of SO_2 from model (left) and RAMA observations (right) at 04:00, 07:00 and 10:00 CDT during the SO_2 plume episode of 10 April 2003. Numbers in brackets show the domain-wide minimum and maximum concentrations of the measurements for the RAMA plots, and of the model area corresponding to the measurement locations for the CAMx plots.

there are 7 of these above 50 ppb during the campaign. By the time they reach CENICA, their impact is reduced except for events occurring during Cold Surge episodes when vertical mixing is low and transport is directly from the north (de Foy et al., 2006a). There are episodes where the model indicates volcanic impacts on the urban area, although these correspond to low SO_2 concentrations. It is therefore difficult to differentiate them from the urban emissions.

Figure 16 shows the comparison in measured and simulated diurnal SO_2 concentrations at CENICA and MER. At CENICA, the morning peak is much more pronounced in the measurements from the monitoring station data than in the DOAS measurements. The simulated concentrations are in reasonable agreement with the DOAS measurements although the morning peak is under-predicted. At MER, levels of SO_2 measured by DOAS are similar to those at CENICA. The simulation levels however are substantially higher suggesting that the spatial distribution of the emission inventory should be re-evaluated for SO_2 in a similar fashion as for CO.

5.3 SO_2 plume event

10 April experienced a large SO_2 plume that swept past the whole city with peak concentrations above 200 ppb in the northern part of the MCMA. Contour plots for 04:00, 07:00 and 10:00 are shown in Fig. 17 for RAMA measurements and model simulations. Figure 18 shows the time series of SO_2 concentrations at points on the northern boundary of the MCMA as well as at different stations along a north–south transect. The initial rise is at TLI, to the west of the Sierra de Guadalupe at around 22:00 of the previous day. Two hours after this there is a substantially larger rise that now extends to VIF to the north, which experiences the bulk of the plume after 03:00. The plume then shifts further east to XAL before returning west to VIF at around sunrise followed by dispersion due to vertical mixing. The impact can be seen at MER building up through the night along with fluctuations due to plume meandering. At CENICA the levels are lower and smoother due to the longer transport distance. This is even more so at PED which starts to see the

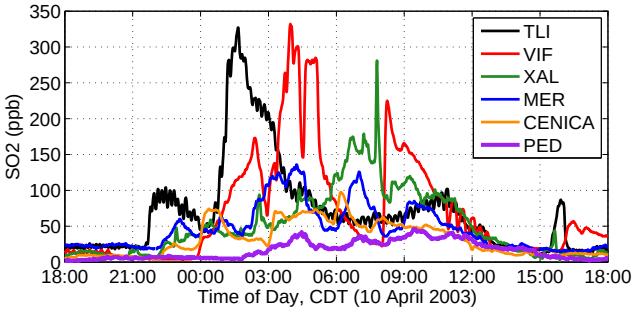

Fig. 18. Time series of measured SO_2 concentrations at 1-min resolution for 10 April plume event at selected RAMA stations and at CENICA.

plume around 03:00 and reaches a maximum between 09:00 and 12:00. Long-path DOAS measurements at CENICA are in remarkable agreement with the point measurement. In addition to adding confidence to the accuracy of the measurements, this highlights the fact that the plume is a large scale phenomenon. Both the measurements and the simulations suggest that the SO_2 plume originated to the north of the MCMA.

As can also be seen in the time series in Fig. 15, the timing and extent of the plume is correctly captured although the maximum levels are under-predicted. The measurement contours show the plume going around both sides of the Sierra de Guadalupe and then moving towards the east. In the model, there is some splitting of the plume around the mountains, but the main effect of the Sierra de Guadalupe is to cause strong vertical mixing leading to a much more diffuse plume. This explains the lower levels observed over the city and the reduced extent of an SO_2-rich air mass separated from the plume moving northeastward at 10:00. This case suggests that the effect of terrain on transport in the stable boundary layer may not be correctly represented numerically.

5.4 Discussion

Both Concentration Field analysis with backward trajectories and forward Eulerian modelling using emission estimates from zenith sky UV spectroscopy suggest that there is a SO_2 plume from the Tula industrial complex that can impact the MCMA. These plumes are typically in the early morning or late evening under stable conditions when wind flows are from the north. While the effect is strongest on the stations in the north of the city, there are occasions where the entire MCMA is affected. Without considering the possible variation in SO_2 emissions, the current simulations captured many of the plumes in the MCMA. The impact on the city is limited to episodes with stable northerly flow. The majority of the time the plume would be expected to follow the prevailing westerlies.

In modelling terms, the SO_2 plume presents a valuable case study for the effect of complex terrain on plume transport under stable conditions. Further study into the vertical dispersion as well as the vertical resolution of the dispersion model could be validated from the surface measurements of SO_2.

Possible impacts from volcanic emissions were identified, although the levels are too low to differentiate from ambient measurements. During the dry season, winds aloft are predominantly westerly and transport the emissions away from the city towards Puebla and beyond. During the field campaign the possible effects were found mainly during the Cold Surge episodes which are characterised by southward winds and stable conditions. It should be noted however that volcanic emissions from the Popocatépetl have been reported to be 10 to 100 times larger than the value used in this study, suggesting that much larger impacts are possible during specific episodes.

Table 3. SO_2 annual emissions estimates from fuel consumption in the MCMA and at the Tula power plant compared with the official inventory for the MCMA and the Mini-DOAS estimate for the Tula industrial complex.

	MCMA	Tula Power Plant
Fuel Consumption (tonne/yr)	5.7×10^6	1.49×10^6
Emission Factor (kg SO_2/tonne fuel)	0.71	86.26
Annual SO_2 Emissions (tonne/yr)	4050	128 000
CAM 2000 Inventory	4929	
Mini-DOAS Estimate		145 000

Annual SO_2 emission estimates for MCMA mobile sources and for the Tula power plant are shown in Table 3. A fleet-average emission factor is derived from long-path DOAS measurements of SO_2 and CO_2 (Volkamer et al., 2005a). Multiplying this by known fuel consumption in the city during April 2003 and scaling to an annual value leads to an emission estimate 20% lower than the official inventory, which is deemed to be within the accuracy of the simulations and the measurements. An estimate of the power plant emissions was obtained by combining the annual fuel consumption and average sulfur content of the fuel. The emissions of the refinery are not included in this estimate. Overall, this is in agreement with the estimate from UV-Spectroscopy plume measurement given the limits of accuracy.

Summing SO_2 impacts at MER and CENICA from model simulations for the Tula and Popocatépetl point sources suggests that in the simulations 75% of SO_2 concentrations are due to local sources during April 2003, with possibly 20% from the power plant and 5% from the volcano.

6 Conclusions

Analysis of CO showed that vertical dispersion schemes in air quality models can have a large impact on simulated

surface concentrations. For the case of CAMx, the scheme of O'Brien (1970) was found to give more realistic results whereas the CMAQ dispersion scheme was overly diffusive.

Column measurements of CO were shown to be a necessary constraint when validating pollutant dispersion models and emissions inventories. Relying on surface measurements alone can lead to compensating errors between the emission levels and the vertical dispersion.

Given the weak and variable winds in the MCMA basin, uncertainties in dispersion simulations can be above 35% and as high as 50%. It is suggested that the current official CO emission inventory is within these error bounds and does not need a large adjustment factor.

Detailed analysis of the spatial and temporal distributions of the measurements and simulations suggest that the spatial distribution of the current emission inventory needs to take into account new urban growth to the north and east of the city. Adjustments by day of week should also be refined to include different temporal profiles both by type of day and by sector of the city.

Concentration field analysis was shown to correctly identify sources of CO irrespective of the monitoring station location. Application of the method to SO_2 shows that large point sources can be identified.

Mini-DOAS measurements of SO_2 plumes was found to be an effective means of measuring emissions from large point sources. Dispersion modelling using the estimated sources was found to be in agreement with surface measurements of the plume, thereby increasing the confidence in the results.

It is suggested that the Tula industrial complex was responsible for some of the large SO_2 peaks observed in the MCMA, but that it only contributes 20% of the long term average concentration. Local sources are the dominant cause of baseline SO_2 levels. Impacts of the Popocatépetl volcano are shown to be possible but could not be differentiated from the local levels.

Measurements of the baseline level of SO_2 are sensitive to interference problems and possible offsets in the monitoring equipment. Comparisons with spectroscopic techniques and/or detailed quality control is needed in order to evaluate the emission inventory and the long term trends in concentrations.

Combined analysis of surface and column CO measurements can serve to evaluate dispersion in air quality models. Large SO_2 plumes provide useful case studies of specific dispersion events. This can contribute to model evaluation. Excessive dispersion was shown for flow past a hill during stable conditions which could serve as a valuable data set for future model development.

The combination of backward Lagrangian trajectories and forward Eulerian modelling can be used to test experiment design and measurement network design. Forward simulations of the urban plume can identify potential measurement sites while backward simulations can identify the regions influencing each monitor.

Carbon monoxide levels are within the health standard at present thanks to reductions in emissions over the last decade, and the current emission inventory was found to give correct CO levels in the dispersion models. Furthermore, CO can be used as a tracer to validate the pollutant transport in numerical models, giving confidence in the results for applications in photochemical and aerosol modelling. The SO_2 health standard is 30 ppb for the annual average with one 24-h average above 130 ppb per year. Currently, this is met for all the stations, but there is the potential for a 24-h average exceedance due to point sources outside the MCMA. It should also be noted that 1-h averages can reach very high levels which are not yet regulated by a health standard. Finally, SO_2 has an impact on aerosol formation and processing, and correctly simulating SO_2 levels is important for future aerosol simulations and their associated health effects.

Acknowledgements. The analysis contained in this paper was made possible by the collaborative efforts of many people involved in field measurements, both during the campaign and over longer periods of time. We are indebted to the staff of CENICA who hosted the campaign. We would like to thank S. Blanco, A. Sanchez, O. Fentanes, J. Zaragoza, A. P. Ocampo, C. Cruz, C. Aguirre, R. Romo, A. Pino, R. Castañeda, R. Rodríguez, P. Escamilla. We would also like to thank C. R. Ramos and the operators and analyst personnel of the "Red Automática de Monitoreo Atmosférico del Gobierno del Distrito Federal" for their contribution in administering and gathering the data used in this manuscript. The valuable reviews from two anonymous referees is gratefully acknowledged.

MM5 is made publicly available and supported by the Mesoscale and Microscale Meteorology division at the National Center for Atmospheric Research for which the authors are very grateful. CAMx is made publicly available by ENVIRON, and the authors would like to thank G. Yarwood and C. Emery for their support. The authors thank A. Stohl for making FLEXPART available and G. Wotawa for developing the MM5 version.

The financial support of the U.S. National Science Foundation, awards ATM-0511803 and ATM-0528227, is gratefully acknowledged.

Edited by: C. E. Kolb

References

Ashbaugh, L. L., Malm, W. C., and Sadeh, W. Z.: A residence time probability analysis of sulfur concentrations at grand-canyon-national-park, Atmos. Environ., 19, 1263–1270, 1985.

Berg, L. K. and Zhong, S. Y.: Sensitivity of MM5-simulated boundary layer characteristics to turbulence parameterizations, J. Appl. Meteorol., 44, 1467–1483, 2005.

Bey, I., Jacob, D. J., Yantosca, R. M., Logan, J. A., Field, B. D., Fiore, A. M., Li, Q. B., Liu, H. G. Y., Mickley, L. J., and Schultz, M. G.: Global modeling of tropospheric chemistry with assimilated meteorology: Model description and evaluation, J. Geophys. Res.-Atmos., 106, 23 073–23 095, 2001.

Biswas, J. and Rao, S. T.: Uncertainties in episodic ozone modeling stemming from uncertainties in the meteorological fields, J. Appl. Meteorol., 40, 117–136, 2001.

Blanchard, C. L.: Methods for attributing ambient air pollutants to emission sources, Annu. Rev. Energy Environ., 24, 329–365, 1999.

Brandt, J., Bastrup-Birk, A., Christensen, J. H., Mikkelsen, T., Thykier-Nielsen, S., and Zlatev, Z.: Testing the importance of accurate meteorological input fields and parameterizations in atmospheric transport modelling using DREAM – Validation against ETEX-1, Atmos. Environ., 32, 4167–4186, 1998.

Byun, D. W.: Dynamically consistent formulations in meteorological and air quality models for multiscale atmospheric studies. Part I: Governing equations in a generalized coordinate system, J. Atmos. Sci., 56, 3789–3807, 1999.

Chow, J. C., Watson, J. G., Edgerton, S. A., Vega, E., and Ortiz, E.: Spatial differences in outdoor PM10 mass and aerosol composition in Mexico City, J. Air Waste Manage. Assoc., 52, 423–434, 2002.

Comisión Ambiental Metropolitana: Inventario de Emisiones de la Zona Metropolitana del Valle de México, Tech. Rep. (Web), Secretaría del Medio Ambiente, Gobierno de México, México, 2004.

de Foy, B., Caetano, E., Magaña, V., Zitácuaro, A., Cárdenas, B., Retama, A., Ramos, R., Molina, L. T., and Molina, M. J.: Mexico City basin wind circulation during the MCMA-2003 field campaign, Atmos. Chem. Phys., 5, 2267–2288, 2005, http://www.atmos-chem-phys.net/5/2267/2005/.

de Foy, B., Clappier, A., Molina, L. T., and Molina, M. J.: Distinct wind convergence patterns in the Mexico City basin due to the interaction of the gap winds with the synoptic flow, Atmos. Chem. Phys., 6, 1249–1265, 2006a.

de Foy, B., Molina, L. T., and Molina, M. J.: Satellite-derived land surface parameters for mesoscale modelling of the Mexico City basin, Atmos. Chem. Phys., 6, 1315–1330, 2006b.

de Foy, B., Varela, J. R., Molina, L. T., and Molina, M. J.: Rapid ventilation of the Mexico City basin and regional fate of the urban plume, Atmos. Chem. Phys., 6, 2321–2335, 2006c.

Delgado-Granados, H., Gonzalez, L. C., and Sanchez, N. P.: Sulfur dioxide emissions from Popocatepetl volcano (Mexico): case study of a high-emission rate, passively degassing erupting volcano, J. Volcanol. Geotherm. Res., 108, 107–120, 2001.

Elias, T., Sutton, A. J., Oppenheimer, C., Horton, K. A., Garbeil, H., Tsanev, V., McGonigle, A. J. S., and Williams-Jones, G.: Comparison of COSPEC and two miniature ultraviolet spectrometer systems for SO2 measurements using scattered sunlight, Bull. Volcanol., 68, 313–322, 2006.

Elliott, S., Blake, D. R., Rowland, F. S., Lu, R., Brown, M. J., Williams, M. D., Russell, A. G., Bossert, J. E., Streit, G. E., Santoyo, M. R., Guzman, F., Porch, W. M., McNair, L. A., Keyantash, J., Kao, C. Y. J., Turco, R. P., and Eichinger, W. E.: Ventilation of liquefied petroleum gas components from the Valley of Mexico, J. Geophys. Res.-Atmos., 102, 21 197–21 207, 1997.

ENVIRON: CAMx, comprehensive air quality model with extensions, User's Guide, Tech. Rep. Version 4.20, ENVIRON International Corporation, 2005.

Fast, J. D. and Zhong, S. Y.: Meteorological factors associated with inhomogeneous ozone concentrations within the Mexico City basin, J. Geophys. Res.-Atmos., 103, 18 927–18 946, 1998.

Fayt, C. and van Roozendael, M.: WinDoas 2.1 – Software User Manual, Tech. rep., IASB/BIRA, Belgium, 2001.

Galle, B., Oppenheimer, C., Geyer, A., McGonigle, A. J. S., Edmonds, M., and Horrocks, L.: A miniaturised ultraviolet spectrometer for remote sensing of SO2 fluxes: a new tool for volcano surveillance, J. Volcanol. Geotherm. Res., 119, 241–254, 2002.

Galle, B., Platt, U., Oppenheimer, C., Millan, M., Alonso, L., and Chen, D.: Development of optical remote sensing instruments for volcanological applications, Tech. Rep. Final Scientific Report on EU-project DORSIVA, Chalmers University of Technology, 2006.

Garcia, A. R., Volkamer, R., Molina, L. T., Molina, M. J., Samuelson, J., Mellqvist, J., Galle, B., Herndon, S. C., and Kolb, C. E.: Separation of emitted and photochemical formaldehyde in Mexico City using a statistical analysis and a new pair of gas-phase tracers, Atmos. Chem. Phys., 6, 4545–4557, 2006, http://www.atmos-chem-phys.net/6/4545/2006/.

Grell, G. A., Dudhia, J., and Stauffer, D. R.: A Description of the Fifth-Generation Penn State/NCAR Mesoscale Model (MM5), Tech. Rep. NCAR/TN-398+STR, NCAR, 1995.

Grutter, M.: Multi-Gas analysis of ambient air using FTIR spectroscopy over Mexico City, Atmosfera, 16, 1–13, 2003.

Grutter, M., Flores, E., Andraca-Ayala, G., and Baez, A.: Formaldehyde levels in downtown Mexico City during 2003, Atmos. Environ., 39, 1027–1034, 2005.

Hong, S. Y. and Pan, H. L.: Nonlocal boundary layer vertical diffusion in a Medium-Range Forecast Model, Mon. Weather Rev., 124, 2322–2339, 1996.

Hopke, P. K.: Recent developments in receptor modeling, J. Chemom., 17, 255–265, 2003.

Jazcilevich, A. D., García, A. R., and Ruiz-Suarez, L. G.: A study of air flow patterns affecting pollutant concentrations in the Central Region of Mexico, Atmos. Environ., 37, 183–193, 2003.

Jazcilevich, A. D., Garcia, A. R., and Caetano, E.: Locally induced surface air confluence by complex terrain and its effects on air pollution in the valley of Mexico, Atmos. Environ., 39, 5481–5489, 2005.

Jiang, G. F., Lamb, B., and Westberg, H.: Using back trajectories and process analysis to investigate photochemical ozone production in the Puget Sound region, Atmos. Environ., 37, 1489–1502, 2003.

Jiang, M., Marr, L. C., Dunlea, E. J., Herndon, S. C., Jayne, J. T., Kolb, C. E., Knighton, W. B., Rogers, T. M., Zavala, M., Molina, L. T., and Molina, M. J.: Vehicle fleet emissions of black carbon, polycyclic aromatic hydrocarbons, and other pollutants measured by a mobile laboratory in Mexico City, Atmos. Chem. Phys., 5, 3377–3387, 2005, http://www.atmos-chem-phys.net/5/3377/2005/.

Jimenez, J. C., Raga, G. B., Baumgardner, D., Castro, T., Rosas, I., Baez, A., and Morton, O.: On the composition of airborne particles influenced by emissions of the volcano Popocatepetl in Mexico, Natural Hazards, 31, 21–37, 2004.

Kolb, C. E., Herndon, S. C., McManus, B., Shorter, J. H., Zahniser, M. S., Nelson, D. D., Jayne, J. T., Canagaratna, M. R., and Worsnop, D. R.: Mobile laboratory with rapid response instruments for real-time measurements of urban and regional trace gas and particulate distributions and emission source characteristics, Environ. Sci. Technol., 38, 5694–5703, 2004.

Kraus, S.: The DOASIS Software, in: 1st International DOAS

Workshop, Heidelberg, Germany, 2001.
Kuhns, H., Knipping, E. M., and Vukovich, J. M.: Development of a United States-Mexico emissions inventory for the Big Bend Regional Aerosol and Visibility Observational (BRAVO) Study, J. Air Waste Manage. Assoc., 55, 677–692, 2005.
Lee, H. N. and Larsen, R. J.: Vertical diffusion in the lower atmosphere using aircraft measurements of Rn-222, J. Appl. Meteorol., 36, 1262–1270, 1997.
Lupu, A. and Maenhaut, W.: Application and comparison of two statistical trajectory techniques for identification of source regions of atmospheric aerosol species, Atmos. Environ., 36, 5607–5618, 2002.
McGonigle, A. J. S., Thomson, C. L., Tsanev, V. I., and Oppenheimer, C.: A simple technique for measuring power station SO2 and NO2 emissions, Atmos. Environ., 38, 21–25, 2004.
Molina, L. T. and Molina, M. J. (Eds.): Air Quality in the Mexico Megacity, Kluwer Academic Publishers, 2002.
Molina, L. T., Molina, M. J., Slott, R., Slott, C. E., Gbor, P. K., Meng, F., Singh, R., Galvez, O., Sloan, J. J., Anderson, W., Tang, X. Y., Shao, M., Zhu, T., Zhang, Y. H., Hu, M., Gurjar, B. R., Artaxo, P., Oyola, P., Gramsch, E., Hidalgo, D., and Gertler, A.: 2004 Critical Review Supplement: Air Quality in Selected Megacities, J. Air Waste Manage. Assoc., p. online only, 2004.
Molina, M. J. and Molina, L. T.: Megacities and atmospheric pollution, J. Air Waste Manage. Assoc., 54, 644–680, 2004.
Nickerson, E. C., Sosa, G., Hochstein, H., Mccaslin, P., Luke, W., and Schanot, A.: Project Aguila – Insitu Measurements of Mexico-City Air-Pollution by a Research Aircraft, Atmos. Environ. B, 26, 445–451, 1992.
Nowacki, P., Samson, P. J., and Sillman, S.: Sensitivity of urban airshed model (UAM-IV) calculated air pollutant concentrations to the vertical diffusion parameterization during convective meteorological situations, J. Appl. Meteorol., 35, 1790–1803, 1996.
O'Brien, J. J.: A note on the vertical structure of the eddy exchange coefficient in the planetary boundary layer, J. Atmos. Sci., 27, 1214–1215, 1970.
Olivie, D. J. L., van Velthoven, P. F. J., and Beljaars, A. C. M.: Evaluation of archived and off-line diagnosed vertical diffusion coefficients from ERA-40 with Rn-222 simulations, Atmos. Chem. Phys., 4, 2313–2336, 2004, http://www.atmos-chem-phys.net/4/2313/2004/.
Olivier, J. G. J. and Berdowski, J. J. M.: Global emissions sources and sinks, in: The Climate System, edited by: Berdowski, J., Guicherit, R., and Heij, B. J., pp. 33–78, A. A. Balkema Publishers/Swets and Zeitlinger Publishers, Lisse, The Netherlands, 2001.
Perez-Roa, R., Castro, J., Jorquera, H., Perez-Correa, J. R., and Vesovic, V.: Air-pollution modelling in an urban area: Correlating turbulent diffusion coefficients by means of an artificial neural network approach, Atmos. Environ., 40, 109–125, 2006.
Platt, U.: Differential Optical Absorption Spectroscopy, in: Monitoring by Spectroscopic Techniques, edited by: Sigrist, M. W., chap. 2, pp. 27–84, Wiley & Sons, New York, 1994.
Raga, G. B., Kok, G. L., Baumgardner, D., Baez, A., and Rosas, I.: Evidence for volcanic influence on Mexico City aerosols, Geophys. Res. Lett., 26, 1149–1152, 1999.
Roelofs, G. J., Scheeren, H. A., Heland, J., Ziereis, H., and Lelieveld, J.: A model study of ozone in the eastern Mediterranean free troposphere during MINOS (August 2001), Atmos. Chem. Phys., 3, 1199–1210, 2003, http://www.atmos-chem-phys.net/3/1199/2003/.
Rothman, L. S., Barbe, A., Benner, D. C., Brown, L. R., Camy-Peyret, C., Carleer, M. R., Chance, K., Clerbaux, C., Dana, V., Devi, V. M., Fayt, A., Flaud, J. M., Gamache, R. R., Goldman, A., Jacquemart, D., Jucks, K. W., Lafferty, W. J., Mandin, J. Y., Massie, S. T., Nemtchinov, V., Newnham, D. A., Perrin, A., Rinsland, C. P., Schroeder, J., Smith, K. M., Smith, M. A. H., Tang, K., Toth, R. A., Auwera, J. V., Varanasi, P., and Yoshino, K.: The HITRAN molecular spectroscopic database: edition of 2000 including updates through 2001, J. Quant. Spectrosc. Radiat. Transfer, 82, 5–44, 2003.
Schifter, I., Diaz, L., Mugica, V., and Lopez-Salinas, E.: Fuel-based motor vehicle emission inventory for the metropolitan area of Mexico city, Atmos. Environ., 39, 931–940, 2005.
Seibert, P., Kromp-Kolb, H., Baltensperger, U., Jost, D. T., and Schwikowski, M.: Trajectory analysis of high-alpine air pollution data, in: Air Pollution Modelling and its Application X, edited by: Gryning, S.-E. and Millan, M. M., pp. 595–596, Plenum Press, New York, 1994.
Sirois, A. and Bottenheim, J. W.: Use of backward trajectories to interpret the 5-year record of pan and o-3 ambient air concentrations at Kejimkujik national park, Nova-Scotia, J. Geophys. Res.-Atmos., 100, 2867–2881, 1995.
Stohl, A.: Trajectory statistics – A new method to establish source-receptor relationships of air pollutants and its application to the transport of particulate sulfate in Europe, Atmos. Environ., 30, 579–587, 1996.
Stohl, A.: Computation, accuracy and applications of trajectories – A review and bibliography, Atmos. Environ., 32, 947–966, 1998.
Stohl, A., Eckhardt, S., Forster, C., James, P., Spichtinger, N., and Seibert, P.: A replacement for simple back trajectory calculations in the interpretation of atmospheric trace substance measurements, Atmos. Environ., 36, 4635–4648, 2002.
Stohl, A., Forster, C., Frank, A., Seibert, P., and Wotawa, G.: Technical note: The Lagrangian particle dispersion model FLEXPART version 6.2, Atmos. Chem. Phys., 5, 2461–2474, 2005, http://www.atmos-chem-phys.net/5/2461/2005/.
Stutz, J. and Platt, U.: Numerical analysis and estimation of the statistical error of differential optical absorption spectroscopy measurements with least-squares methods, Appl. Opt., 35, 6041–6053, 1996.
Ulke, A. G. and Andrade, M. F.: Modeling urban air pollution in Sao Paulo, Brazil: sensitivity of model predicted concentrations to different turbulence parameterizations, Atmos. Environ., 35, 1747–1763, 2001.
Vandaele, A. C., Simon, P. C., Guilmot, J. M., Carleer, M., and Colin, R.: SO2 absorption cross-section measurement in the UV using a fourier-transform spectrometer, J. Geophys. Res.-Atmos., 99, 25 599–25 605, 1994.
Vasconcelos, L. A. D., Kahl, J. D. W., Liu, D. S., Macias, E. S., and White, W. H.: A tracer calibration of back trajectory analysis at the Grand Canyon, J. Geophys. Res.-Atmos., 101, 19 329–19 335, 1996a.
Vasconcelos, L. A. D., Kahl, J. D. W., Liu, D. S., Macias, E. S., and White, W. H.: Spatial resolution of a transport inversion technique, J. Geophys. Res.-Atmos., 101, 19 337–19 342, 1996b.
Volkamer, R., Molina, L. T., Molina, M. J., Flores, E., Grutter, M., Galle, B., Mellqvist, J., Samuelsson, J., Knighton, B., and Job-

son, B. T.: Open-path emission factors derived from DOAS and FTIR measurements in the Mexico City Metropolitan Area, in: Air Pollution as a Climate Forcing: A Second Workshop, 2005a.

Volkamer, R., Molina, L. T., Molina, M. J., Shirley, T., and Brune, W. H.: DOAS measurement of glyoxal as an indicator for fast VOC chemistry in urban air, Geophys. Res. Lett., 32, doi:10.1029/2005GL022616, 2005b.

West, J. J., Zavala, M. A., Molina, L. T., Molina, M. J., San Martini, F., McRae, G. J., Sosa-Iglesias, G., and Arriaga-Colina, J. L.: Modeling ozone photochemistry and evaluation of hydrocarbon emissions in the Mexico City metropolitan area, J. Geophys. Res.-Atmos., 109, doi:10.1029/2004JD004614, 2004.

Williams, M. D., Brown, M. J., Cruz, X., Sosa, G., and Streit, G.: Development and testing of meteorology and air dispersion models for Mexico City, Atmos. Environ., 29, 2929–2960, 1995.

Yurganov, L. N., Blumenstock, T., Grechko, E. I., Hase, F., Hyer, E. J., Kasischke, E. S., Koike, M., Kondo, Y., Kramer, I., Leung, F. Y., Mahieu, E., Mellqvist, J., Notholt, J., Novelli, P. C., Rinsland, C. P., Scheel, H. E., Schulz, A., Strandberg, A., Sussmann, R., Tanimoto, H., Velazco, V., Zander, R., and Zhao, Y.: A quantitative assessment of the 1998 carbon monoxide emission anomaly in the Northern Hemisphere based on total column and surface concentration measurements, J. Geophys. Res.-Atmos., 109, D15305, 2004.

Yurganov, L. N., Duchatelet, P., Dzhola, A. V., Edwards, D. P., Hase, F., Kramer, I., Mahieu, E., Mellqvist, J., Notholt, J., Novelli, P. C., Rockmann, A., Scheel, H. E., Schneider, M., Schulz, A., Strandberg, A., Sussmann, R., Tanimoto, H., Velazco, V., Drummond, J. R., and Gille, J. C.: Increased Northern Hemispheric carbon monoxide burden in the troposphere in 2002 and 2003 detected from the ground and from space, Atmos. Chem. Phys., 5, 563–573, 2005, http://www.atmos-chem-phys.net/5/563/2005/.

Zavala, M., Herndon, S. C., Slott, R. S., Dunlea, E. J., Marr, L. C., Shorter, J. H., Zahniser, M., Knighton, W. B., Rogers, T. M., Kolb, C. E., Molina, L. T., and Molina, M. J.: Characterization of on-road vehicle emissions in the Mexico City Metropolitan Area using a mobile laboratory in chase and fleet average measurement modes during the MCMA-2003 field campaign, Atmos. Chem. Phys., 6, 5129–5142, 2006, http://www.atmos-chem-phys.net/6/5129/2006/.

Zhong, S. Y. and Fast, J.: An evaluation of the MM5, RAMS, and Meso-Eta models at subkilometer resolution using VTMX field campaign data in the Salt Lake Valley, Mon. Weather Rev., 131, 1301–1322, 2003.